From seismic noise to ocean wave parameters: General methods and validation

Fabrice Ardhuin,[1] Abel Balanche,[1] E. Stutzmann,[2] and Mathias Obrebski[1]

Received 14 July 2011; revised 29 February 2012; accepted 12 March 2012; published 1 May 2012.

[1] Seismic noise is an indirect source of information on ocean waves. Using a model of noise generation and propagation, seismic stations can be separated into those that are mostly sensitive to local sea states, and those that integrate sources from a large oceanic area. The model also provides a classification of noise-generating sea states into three classes. The analysis of Central California seismic noise data, well correlated with local waves, reveals that class I events dominate in summer, caused by a single wind-sea system, and for which ocean wave spectral levels are proportional to seismic spectral levels to an exponent $b \simeq 0.9$. In winter, noise is dominated by class II generation, for which coastal reflection is important, with a wave spectral density roughly proportional to the seismic spectral density to an exponent $b \simeq 0.7$. Sporadic events of class III probably produce some of the strongest noise events in Central California and need to be properly screened. These events are caused by opposed wave systems that are usually the wind-sea and a swell. This noise classification can be used to improve on the correlation between measured and estimated wave heights (up to $r = 0.93$ for daily averages). For other locations, where remote oceanic sources are recorded, a significant wave height estimated from the seismic noise compares well with area-averaged satellite data or wave model results ($r > 0.85$ for daily averages). These analyses pave the way for quantitative uses of seismic records, including the reconstruction of past wave climates, and the calibration of wave hindcasts.

Citation: Ardhuin, F., A. Balanche, E. Stutzmann, and M. Obrebski (2012), From seismic noise to ocean wave parameters: General methods and validation, *J. Geophys. Res.*, *117*, C05002, doi:10.1029/2011JC007449.

1. Introduction

[2] Since the early days of seismology, the ubiquitous noise with periods 5 to 10 s has been clearly associated to ocean wave activity (for a historical account, see *Bernard* [1990]). The corresponding ground motions have vertical excursions of the order of a few micrometers, hence their usual name microseisms. The detailed relationship between microseisms and ocean waves was only clarified much later with the observation by *Bernard* [1941] that the dominant frequency of microseisms is the double of the dominant ocean wave frequencies and follows its changes, suggesting that partial standing waves could be the origin of the recorded noise. The theoretical works of *Miche* [1944] on the pressure induced by partially standing waves was the missing link that led *Longuet-Higgins* [1950] to propose the first plausible theory of seismic noise generation as seismic Rayleigh waves generated by surface gravity waves in deep water. The theory was generalized to random waves by *Hasselmann* [1963].

[3] The lack of a theoretical understanding did not prevent various propositions for using seismic noise as a source of information on ocean storms and weather, or for wave forecasting [*Algué*, 1900; *Bernard*, 1937], and a practical use of wave-measuring devices based on seismometers eventually emerged [*Zopf et al.*, 1976]. Yet, by the 1980s, ocean technology allowed routine wave measurements by buoys at sea, making the seismic 'wavemeter' almost obsolete. Further, satellite altimeters and synthetic aperture radars have provided routine and accurate measurements over the entire globe since 1991 [e.g., *Tournadre and Ezraty*, 1990; *Collard et al.*, 2009]. The coarse space-time and spectral coverage provided by satellites leaves an important potential use for seismometer-based techniques in areas where in situ measurements are inexistent or not available [e.g., *Barruol et al.*, 2006]. The presence of low-frequency energy in seismic records is a clear indication of long period waves associated with the most severe storms, as shown by *Ebeling and Stein* [2011] and *Hanafin et al.* [2012] and can be used to investigate extreme wave events. Also numerical wave models need to be corrected for time-dependent biases that are caused by the time-dependent errors in the winds used as input [e.g., *Caires and Sterl*, 2005].

[1] Ifremer, Laboratoire d'Océanographie Spatiale, Plouzane, France.
[2] Departement de Sismologie, Institut de Physique du Globe, PRES Sorbonne Paris-Cité, Paris, France.

Copyright 2012 by the American Geophysical Union.
0148-0227/12/2011JC007449

[4] Finally, seismic noise is related to the poorly known directional distribution of wave energy [e.g., *Farrell and Munk*, 2008], and is also uniquely sensitive to very long period swells and their fore-runners, with periods longer than 20 s, that are the fingerprints of the most severe storms [*Munk et al.*, 1963; *Delpey et al.*, 2010]. There is thus a need for understanding the seismic data for the analysis of ocean wave properties.

[5] Beyond the estimation of present sea states, the reconstruction of past time series of ocean wave parameters has emerged as a new possible application. Old seismographs go back to the early 20th century, which is 80 years before our modern age of space-based measurements of ocean waves. *Bernard* [1981, 1990] analyzed seismic noise variability at stations around the North Atlantic, from 1906 to 1980, to find evidence of a solar cycle in the the storm climate. He concluded that there is an 11-year cycle in the seismic noise. Looking at his time series with our modern eyes, we rather see a correlation of noise levels with the North Atlantic Oscillation index. Unfortunately details about the seismic data processing are missing to further verify that work. This quest for a quantitative link between wave climate and seismic noise has been taken up by others, with noteworthy efforts by *Bromirski et al.* [1999] for California, and *Essen et al.* [1999] for the North-East Atlantic, while the analysis of many seismic records around the word indicate upward trends in seismic noise levels that was interpreted as an increase in ocean wave heights [*Aster et al.*, 2010]. Based on ocean wave buoy measurements, some skill was shown for the reconstruction of time series of the significant wave height (H_s) over a few month period for Central California. the correlation was probably $r(H_s) > 0.8$ for hourly time series, with Pearson's linear correlation for a quantity X defined by

$$r(X) = \frac{\sum \left(X_{\rm obs} - \overline{X_{\rm obs}}\right)\left(X_{\rm mod} - \overline{X_{\rm mod}}\right)}{\sqrt{\sum \left(X_{\rm obs} - \overline{X_{\rm obs}}\right)^2 \left(X_{\rm mod} - \overline{X_{\rm mod}}\right)^2}}, \qquad (1)$$

where the overbar denotes the arithmetic average, and $X_{\rm obs}$ and $X_{\rm mod}$ are the observed and modeled series.

[6] For the North Atlantic, a numerical wave model was used to find a significant correlation ($r = 0.71$) for 6-hourly time series between winter waves in various regions of the North-East Atlantic, and noise levels at the Hamburg seismic station [*Essen et al.*, 1999]. Yet, with that correlation, seismic noise explains only half of the wave model variance ($r^2 = 0.5$), and this was only applied to winters. It is thus premature to use results of these earlier studies to conclude on the general feasibility of wave estimation at other locations. Further, the retrieval of sea state parameters is not guaranteed beyond the seasonal time series that were studied. Thus, either for present-day or historical wave reconstruction, there is a clear need for defining the conditions in which wave parameters can be estimated from seismic data, and to explore the systematic differences in sea states that may yield different seismic responses.

[7] The goal of the present paper is to extend these previous studies toward robust and generic methods for estimating sea state parameters from seismic noise. For this, we build upon the recent improvement in numerical wave models [*Cavaleri et al.*, 2007; *Ardhuin et al.*, 2010], and the resulting good performance of a direct model of seismic noise. Seismic noise model results are well correlated with observed root mean square vertical ground displacements amplitudes. *Ardhuin et al.* [2011a] (hereinafter ASSM) obtained correlations higher than 0.85 for 4-hourly seismic data over the entire year. *Schimmel et al.* [2011] also independently verified the location of the sources with the measured polarization directions of Rayleigh waves. This model may thus be used to guide the interpretation of seismic noise records, especially for estimating the locations of the noise sources and thus the locations where sea state parameters may be retrieved. However, this kind of model does not include three-dimensional seismic propagation effect and may fail to explain the noise recorded at some seismic stations. In particular, it is important to recognize that several publications, most conspicuously the analysis of typhoon Ioke by *Zhang et al.* [2010, Figure S2] failed to find evidence of seismic noise propagation as surface (Rayleigh) waves from deep water to land. Along this line, many published analyses of seismic data interpret high noise levels from some direction that intersects the coastline as evidence for the importance of the coast in the generation of this noise [*Bromirski et al.*, 2005; *Gerstoft and Tanimoto*, 2007; *Traer et al.*, 2008]. Others interpreted their measurements as evidence of this deep water to land propagation [*Cessaro*, 1994; *Chevrot et al.*, 2007; *Kedar et al.*, 2008; *Ardhuin et al.*, 2011a]. From observations alone it is clearly impossible to decide on the position of one or several sources along a great circle in a given back-azimuth. This is where a numerical model provides interesting additional quantitative information by estimating the plausible energy levels of the sources at each point in the ocean. Because of that controversy, we discuss below the quality of the ASSM model and the resulting uncertainties on the location of modeled noise sources. Our numerical model supports that there are plausible sources of Rayleigh waves generated in deep water that occasionally dominate the signal recorded at land-based stations, including stations in California. These modeled deep sources occur systematically at the same time as the largest outliers in the correlation of wave heights and seismic noise levels. We shall thus use these modeled sources as a proxy for outliers in order to reduce our errors on wave height estimation.

[8] After a review of the underlying theory in section 2, we will discuss, in section 3, why and how seismic noise correlates with sea state parameters for seismic stations dominated by nearshore seismic noise sources, with or without wave reflection at the shoreline. In section 4 we explore the case of seismic stations that record noise generated in large areas. In both cases we propose a method for the reconstruction of time series of the significant wave height.

2. Wave-Noise Relations Expected From Theory

2.1. General Considerations

[9] Ocean waves are known to generate microseisms via at least two distinct generation mechanisms. Primary microseisms, with a frequency equal to the ocean wave frequency, are only generated on sloping shallow topography in coastal areas [*Hasselmann*, 1963]. Here we only consider the secondary microseisms, which are far more energetic and

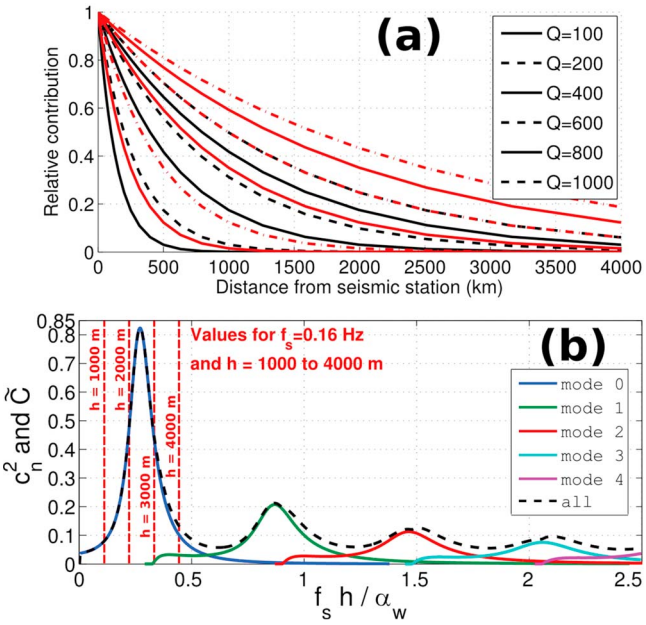

Figure 1. (a) Relative contributions of sources at various distances, in the case of a spatially uniform source distribution for f_s = 0.2 Hz in black, and f_s = 0.12 Hz in red. (b) Non-dimensional coefficient $\tilde{C}$ defined by equation (4), as a function of the non-dimensional depth $f_s h/\alpha_w$ which is equal to the ratio of water depth over acoustic wavelength.

generated over large regions of the ocean. They appear when ocean wave trains with nearly opposite directions and identical frequency f are superimposed [*Longuet-Higgins*, 1950; *Hasselmann*, 1963], which makes noise at the double frequency (DF) $f_s = 2f$.

[10] Following ASSM, we neglect changes in seismic group velocity U along their propagation path. We further assume that seismic waves are damped with a quality factor Q, such that, for a given seismic station, UQ is a constant for all the dominant seismic modes recorded by a given seismometer.

[11] The seismic noise power spectrum F_δ recorded on the vertical component at a station of longitude λ and latitude ϕ on the Earth's surface is given by the directional wave spectra over the ocean at all positions (λ', ϕ') through the source $S_{DF}(f_s)$. With Δ the spherical distance between source and station, and R_E the Earth radius, it is

$$F_\delta(\lambda,\phi,f_s) = \int_\Omega \frac{S_{DF}(\lambda',\phi',f_s)P(\lambda',\phi',f_s)}{R_E \sin\Delta}\, e^{-2\pi f_s \Delta R_E/(UQ)} dA, \quad (2)$$

where $dA = R_E^2 \cos\phi'\, d\lambda' d\phi'$ is the elementary area of the ocean surface Ω. Finally $P(\lambda', \phi', f_s)$ is an empirical correction factor for three-dimensional propagation effects. When $P = 1$ as in ASSM, the propagation of the seismic (Rayleigh) waves correspond to a vertically symmetric earth model. Several measurements with pairs of nearby stations, one on land and the other at the bottom of the ocean, have shown that the noise recorded on land can be much weaker than that recorded at the ocean bottom [*Bromirski and Duennebier*, 2002; *Webb and Crawford*, 2010]. This suggests that for land stations P is generally less than unity, probably due to the refraction of seismic waves by the ocean-continent gradient in phase speed as well as change in group speed and ratio of energy to surface ground variance [e.g., *Hasselmann*, 1963].

[12] The prominence of distant versus local sources is controlled by the geometrical spreading factor 1/sin Δ and, more importantly, by the magnitude of Q. For high Qs, seismic sources from large distances can be recorded, while low Qs reduce the typical distance from which sources can be recorded. For example, taking f_s = 0.15 Hz, U = 1800 m/s and a low value of Q = 100, the seismic energy is reduced by a factor 2 every 130 km. This distance is proportional to Q, and thus a high value Q = 800 will yield a significant contribution from more remote sources (Figure 1a).

[13] The local source of seismic noise $S_{DF}(f_s)$ is the contribution to the vertical ground displacement spectral density, per unit distance of propagation of the seismic waves [*Hasselmann*, 1963] (equations 1–5 in ASSM). This source can be expressed from the frequency-directional ocean wave spectrum $F(f, \theta)$ which is often expressed as a product of the frequency spectrum $E(f)$ times an angular distribution function $M(f, \theta)$

$$F(f,\theta) = E(f)M(f,\theta), \quad (3)$$

where θ are the wave propagation directions.

[14] For ease of reading, the dependence of the seismic source on λ' and ϕ' is now implicit as we only consider the local wave and seismic response properties.

[15] The local conversion from ocean waves to seismic Rayleigh waves is a function of the ratio of sound wavelength and water depth, represented by a non-dimensional coefficient $\tilde{C}$,

$$\tilde{C} = \sum_{n=0}^{N} c_n^2. \quad (4)$$

We obtained the mode coefficients c_n, as defined by *Longuet-Higgins* [1950], by following the procedure outlined by *Hasselmann* [1963], which involves solving for the coupling of ocean waves and seismic waves with a uniform ocean and semi-infinite crust. Here the model was applied with N = 1, i.e. keeping only the first two modes. Figure 1b shows that for a given frequency, only a narrow range of depths gives a very strong response.

[16] For ocean waves of periods 8 to 16 s, noise generation is several times larger at depths in the range 1500 to 3000 m compared to water depths less than 500 m or more than 4000 m. Taking constant water and crust densities ρ_w = 1000 kg m^{-3} and ρ_s = 2500 kg m^{-3}, the source is

$$S_{DF}(f_s) \simeq \rho_w^2 g^2 \frac{2\pi f_s^2 \tilde{C}}{\rho_s^2 \beta^5} E^2(f) I(f), \quad (5)$$

where β = 3000 m s^{-1} is the crust shear wave velocity, also assumed constant. $I(f)$ is a non-dimensional function that depends only on $M(f, \theta)$,

$$I(f) = \int_0^\pi M(f,\theta)M(f,\theta+\pi)d\theta. \quad (6)$$

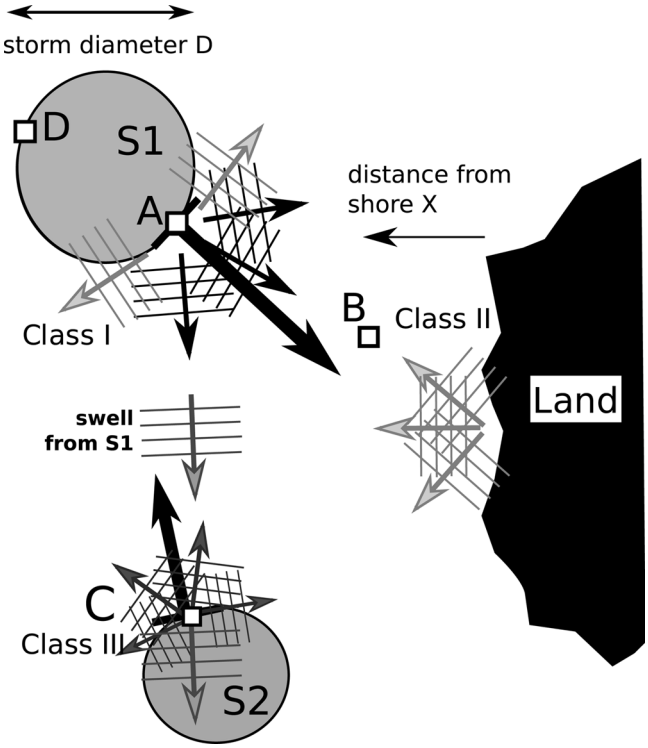

Figure 2. Schematic of the three classes of seismic noise generation events. The thick arrows indicate the local wind direction and the small arrows indicate the direction of wave trains. At point A, in the storm S1, the local wind-sea spectrum is broad enough by itself to contain energy in opposite wave trains, that propagate in directions greater than 90 degrees from the wind direction, capable of generating a measurable seismic noise (class I). At point B, wind waves generated by storm S1 interact with their reflection from shore (class II). At point C, remote swells from storm S1 run into wind seas from storm S2 (class III).

This directional integral means that there will be noise if and only if there is some energy in opposite directions θ and $\theta + \pi$ and at the same frequency f.

2.2. Refinement of the Pelagic and Coastal Source Classification Into Three Classes

[17] Due to the necessary presence of waves in opposing directions, only specific sea states can yield significant levels of seismic noise. Until recently, two main types of sources had been considered, generally termed 'pelagic' and 'coastal' sources. Here we rather follow the terminology of ASSM. Taking that classification backwards, for a more simple description, class III corresponds to the events in which two wave systems of distinct origin but equal wave periods run into one another, these are most typically one swell from a remote source with a locally generated wind sea [e.g., *Kedar et al.*, 2008, Figure 2], but can also be two swells from two remote sources. The two storms do not need to exist at the same time, but waves from one, when traveling at the group velocity, must cross the trajectory of waves from the other (Figure 2).

[18] The other usual source occurs at or near any reflecting ocean boundary, usually the coasts, at mainlands or islands, we will call this class II. The noise generated in this case can actually come from deep water because part of the reflected wave energy propagates back across the open ocean. In practice, significant reflection can also occur in the marginal ice zone or around icebergs [*Squire et al.*, 1995; *Ardhuin et al.*, 2011b]. Wave scattering over bottom topography may also produce opposing wave trains [*Ardhuin and Magne*, 2007], but it only occurs in shallow water, where the conversion of wave-induced pressure to seismic noise is very weak. Conversely, wave refraction or scattering by current gradients may broaden the wavefield in deep water [*Holthuijsen and Tolman*, 1991; *Fabrikant and Raevsky*, 1994; *Lavrenov*, 2003a], and contribute to seismic noise.

[19] Based on their numerical model, ASSM proposed that the most common source in the 0.1 to 0.3 Hz seismic frequency band, albeit weak, is generated by a single wind sea system. Indeed, because of the nonlinear evolution of random waves [e.g., *Lavrenov*, 2003b; *Cavaleri et al.*, 2007], the directional spectrum has a very broad directional distribution, especially at frequencies a few times higher or lower than the peak frequency, so that there is always some energy in opposite directions that generate seismic noise. ASSM designated these sources as class I. Namely, noise can be generated by a perfectly stationary and uniform wind, not necessarily in a cyclonic storm as originally proposed by *Longuet-Higgins* [1950]. This property has received little attention so far, except for high frequency waves [*Farrell and Munk*, 2008, 2010; *Duennebier et al.*, 2012].

[20] From high frequency radar observations the energy of opposing wave trains can be estimated for wavelengths of a few tens of meters and shorter, corresponding to wave frequencies higher than 0.25 Hz [*Crombie*, 1955]. For longer waves, closer to the peak frequency, recent detailed directional wave measurements suggest that the wave spectrum is indeed broad enough [*Long and Resio*, 2007] to generate a significant level of noise.

[21] From a wave modeling point of view, the clean separation of seismic sources, into those due to reflection and the others, is practically impossible and meaningless. Indeed, in the Longuet-Higgins-Hasselmann theory, the noise source is always determined from the directional ocean wave spectrum, whatever the reason for the existence of opposing wave trains. Yet, the relative amplitude of the two opposing wave trains should vary with the cause for their existence, and we show below that different causes can produce different relationships between seismic and ocean wave spectra.

2.3. Noise Level and Directional Wave Spreading

[22] The overlap integral $I(f)$ in equation (5) can be estimated from pressure records at depths from 15 to 300 m [*Herbers and Guza*, 1994; *Cox and Jacobs*, 1989] but, unfortunately, it cannot be measured by conventional wave buoys. However, buoys provide a measure of the directional spreading $\sigma_1(f)$ which is a measure of the width of $M(f, \theta)$ [e.g., *Kuik et al.*, 1988],

$$\sigma_1(f) = \sqrt{2[1 - m_1(f)]}, \quad (7)$$

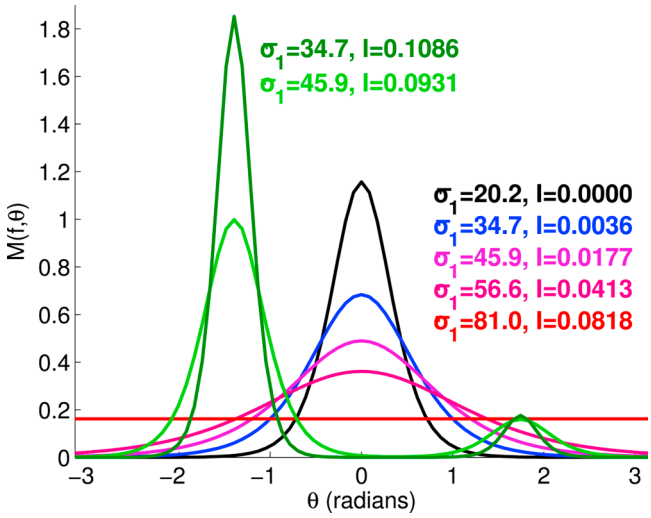

Figure 3. Examples of directional distributions and associated values of the overlap integral I and the directional spreading σ_1. The area below all curves is the same, equal to 1. For the five distributions M centered on 0, we have used the same parametric form $M(\theta) \propto 1/\cosh^2[B(\theta - \theta_0)]$, for which I increases monotonically with σ_1. For the other two distributions, in green, we have combined this same distribution around opposite directions. These two distributions have values of σ_1 and I that vary with opposite trends: when the two peaks become narrower, I increases.

where the first directional moment is

$$m_1(f) = \int_0^{2\pi} M(f,\theta)\cos[\theta - \theta_0(f)]\mathrm{d}\theta, \tag{8}$$

with $\theta_0(f)$ the mean wave direction at frequency f. For a narrow spectrum, $\sigma_1(f)$ is the standard deviation (the half-width) of the distribution $M(f, \theta)$.

[23] As illustrated by Figure 3 and discussed in ASSM, $I(f)$ can vary by several orders of magnitude with changes in the directional distribution $M(f, \theta)$, even if $E(f)$ remains the same. This variation forbids direct and generic relationships between the significant oceanic wave height

$$H_s = 4\sqrt{\int_0^{\infty} E(f)\mathrm{d}f} \tag{9}$$

and the seismic sources. Namely, a strong source can occur with a relatively low wave height, and a very large wave height may give a weak seismic source. In fact σ_1 and I may also vary differently for arbitrary shapes of M. Still, $I(f)$ and $\sigma_1(f)$ can be related to $E(f)$ for a majority of real spectral shapes.

2.4. Class I Generation

[24] Here we consider noise generated by wind-sea waves only, that are forced by the local wind, assumed uniform. Following the details in the appendix A, the seismic source in equation (2) can be re-written as equation (A1) and we may parameterize the directional integral $I(f)$ from the wave power spectrum $E(f)$, giving a relationship between $E(f)$ and the seismic noise spectrum $F_\delta(2f)$ in the form

$$E(f) \simeq a(f)[F_\delta(f_s)]^{b(f)}. \tag{10}$$

The frequency-dependent coefficients a and b represent a proportionality coefficient, and an exponent that define a transfer function from the seismic spectrum to the wave spectrum. If the directional integral $I(f)$ had been constant, we would have $b = 0.5$. However, as detailed in Appendix A, we expect $b > 0.5$ because $I(f)$ generally decreases when $E(f)$ increases.

2.5. Class II Generation

[25] When coastal reflections are the sources of the opposite wave trains, we may also simplify the noise model, as proposed by *Bromirski et al.* [1999].

[26] Assuming that reflection is linear, a narrow incident wavefield from direction θ_m produces a back-scattered wavefield in the opposite direction $\theta_m + \pi$, with a spectral density of the reflected waves reduced by a factor $R_o^2(f, \theta_m)$ compared to the incident waves (see Appendix B for details). For a wavefield that varies on scales much larger than the seismic attenuation scale $UQ/(2\pi f_s)$, the recorded seismic spectrum is then given by

$$F_\delta(\lambda,\phi,f_s) \simeq R_o^2(f,\theta_m)E^2(f)\int_{-\pi/2}^{\pi/2}\int_0^{2\pi}\frac{2\pi f_s \tilde{C}\rho_w^2 g^2 f_2}{\rho_s^2\beta^5 R_E\sin\alpha} \times \mathrm{e}^{-2\pi f_s \alpha R_E/(UQ)}\mathrm{d}A. \tag{11}$$

The integral is a function of the wave frequency only, similar to *Bromirski et al.* [1999, equation 5].

[27] We thus attempt to invert equation (11) in the form

$$E(f,t) \simeq a(f,\theta_m)[F_\delta(f_s, t+\tau)]^{b(f,\theta_m)}, \tag{12}$$

where a and b are empirical coefficients that we will determine, and τ is a time shift that accounts for the travel time of waves from the center of the seismic generation area to the shoreline and back.

[28] For a linear reflection one would find $b = 0.5$, as used by *Bromirski et al.* [1999], but we expect $b > 0.5$ because reflection is not linear. Indeed, the wave reflection coefficient is defined from the wave amplitudes outside of the surf zone, whereas reflection mostly occurs within the surf zone, after the wave height has been reduced by breaking. As a result, the reflection coefficient decreases when the incident wave energy increases [*Elgar et al.*, 1994; *O'Reilly et al.*, 1999].

2.6. Class III Generation: Interaction of Two Wave Systems

[29] In this case, noise is produced by one swell system and the wind-sea, driven by the local wind, or two swells. The noise source is now proportional to $E_1(f)E_2(f)I(f)$ where $E_1(f)$ and $E_2(f)$ are the spectral densities of the two interacting wave systems, and $I(f)$ is the directional integral which depends on the exact mean directions and spreads of the two wave systems. These events can produce a much stronger noise than classes I or II for a given significant

wave height. *Zopf et al.* [1976] already noted that, on the Oregon coast, offshore winds could produce seismic noise levels that would otherwise have been caused by waves twice as large.

[30] For classes I and II the energy levels of the opposing wave trains are related, but this is generally not the case in class III events. We expect some trends of increasing noise with increasing wave heights, in particular in the special case when the swell was generated by the same moving storm, as discussed by *Haubrich and McCamy* [1969]. One could also imagine that a background swell of more or less constant properties will allow the noise generated to be proportional to the energy of the wind sea. These relationships, however, are expected to exhibit a lot of scatter because the amplitude of swells running against a wind sea (or another swell) with the same frequency can be anything from 1 cm to 10 m.

3. Example of Noise From Local Sources: The Berkeley Record and Central California Waves

[31] We may now estimate the local wave spectrum, offshore of San Francisco, using data from Berkeley seismic station (BKS), as done by *Bromirski et al.* [1999], and compare it to that measured by the U.S. National Data Buoy Center buoy number 46013. Indeed, the analysis of the BKS by ASSM suggests that the seismic noise is attenuated with a damping factor Q of the order of 90–300, with possible even higher values at the lowest frequencies.

[32] This implies a localization of most of the seismic sources within a 150 to 250 km wide strip that extends from 36° to 45° N, from the shelf break toward the open ocean (the 50% contour in Figures 4b and 4c). The shape of this dominant source region is largely controlled by the depth-dependent amplification coefficient $\tilde{C}$ in equation (2), as shown in Figure 1b, with a maximum located between 2000 and 3000 m depth for f_s = 0.14 Hz, which is the peak frequency of the annual average seismic spectrum at BKS. Likewise, the sharp increase of the source level when crossing the Mendocino fracture zone northbound, at 40° N, is related to the shallower depth of the ocean bottom in that area. The source area has a rather large extent, and probably 5 to 20% of the noise energy is generated north of Cape Mendocino. Such remote coastal sources have been identified by *Bromirski and Duennebier* [2002]. These sources certainly contribute to the scatter in our estimation of local wave parameters because the sea state in that area is only weakly correlated to the sea state at the 46013 buoy. For example, using 3-hourly data for the year 2008, the correlation of H_s recorded at the buoy 46050 (located 30 km from shore at 44° N) with the record at 46013 is r = 0.47 for the full frequency band but r = 0.74 for wave frequencies below 0.75 Hz.

3.1. Seismic Data Processing

[33] We processed seismic records into 4-hour blocks by averaging spectra obtained over 512 s segments. The seismic data are shifted τ = 2 hours back in time, which corresponds to a propagation of 70 km for waves with a period of 12 s, consistent with the location of the source maximum in the ASSM noise model, within 100 km from shore. *Bromirski et al.* [1999], found that this time shift actually maximizes the correlation of the energy levels in ocean wave and seismic noise.

[34] The resulting spectra are averaged to a seismic frequency resolution of 0.01 Hz for f_s < 0.2 Hz and 0.02 Hz otherwise, so that one frequency band from the buoy corresponds to one frequency band from the seismometer, at the double frequency and with a double bandwidth. This processing effectively averages 144 spectra for each band, thus the spectrum is estimated with 288 degrees of freedom, and an expected accuracy of ± 16% (± 0.6 dB) at the 95% confidence level [e.g., *Donelan and Pierson*, 1983]. The buoy data are similarly averaged over 4 hours but it consists of a succession of 20 minute records for each hour, which gives only 48 degrees of freedom at a resolution of 0.005 Hz and an expected random error of ± 40% (± 1.5 dB). Buoy data are thus intrinsically more noisy than the seismic record.

[35] In order to filter out Earthquakes and seismometer glitches, we have adapted the procedure described in ASSM, now filtering each frequency band separately.

[36] Namely, a spectral density was discarded when it jumped by a factor 10 or more over 4 hours. Here we integrated spectral wave parameters over the frequency band 0.05 to 0.18 Hz. As a result, for any time record, any missing spectral density in the seismic frequency band 0.1 to 0.36 Hz resulted in the full record being discarded.

3.2. Wave Reconstruction Methods Without Classification

[37] We now attempt to retrieve the ocean wave frequency spectrum $E(f)$ from the seismic noise spectrum $F_\delta(f_s)$, for $f_s = 2f$. This inversion of equation (2), uses the empirical equation (10) in which the constants a and b are fitted. We first examine the correlation of the ocean wave and seismic spectral densities that we are trying to associate.

[38] Looking at wave measurements from buoy 46013 on Figure 5, $E(f)$ appears well correlated with $F_\delta(f_s)$, for f between 0.07 and 0.23 Hz. Similar results are obtained with buoy 46214 (for locations, see Figure 4). The uncertainty of the spectral estimates, 1.4 dB for the wave spectra, is clearly less than the scatter in the seismic-to-wave relationships shown in Figure 5. There are signs that different wave directions result in different seismic energy levels. At the higher frequencies in Figure 5, a cloud of orange dots stand out with wave energies relatively higher than that of blue dots that have the same seismic spectral density. These orange dots correspond to waves with a mean direction between 320 and 340 that propagate almost alongshore and for which reflection is expected to be weaker, giving a weaker seismic noise. However, this trend is not very clear, and could also be contaminated by remote sources. We will thus ignore the possible dependence of a and b on θ_m.

[39] There are, in general, a significant number of outliers with low wave energy. These are likely due to non-local seismic sources that dominate the BKS record when the local waves are very small. We therefore exclude the lowest 10% values of $E(f)$ and fit a linear relationship between the logarithms of the two spectral densities, as illustrated by the solid lines in Figure 5. The fitted slopes give an exponent b that is systematically greater than 0.5, as expected from our analysis in section 2. That larger b will increase the range of our estimates of wave energy. The equivalent

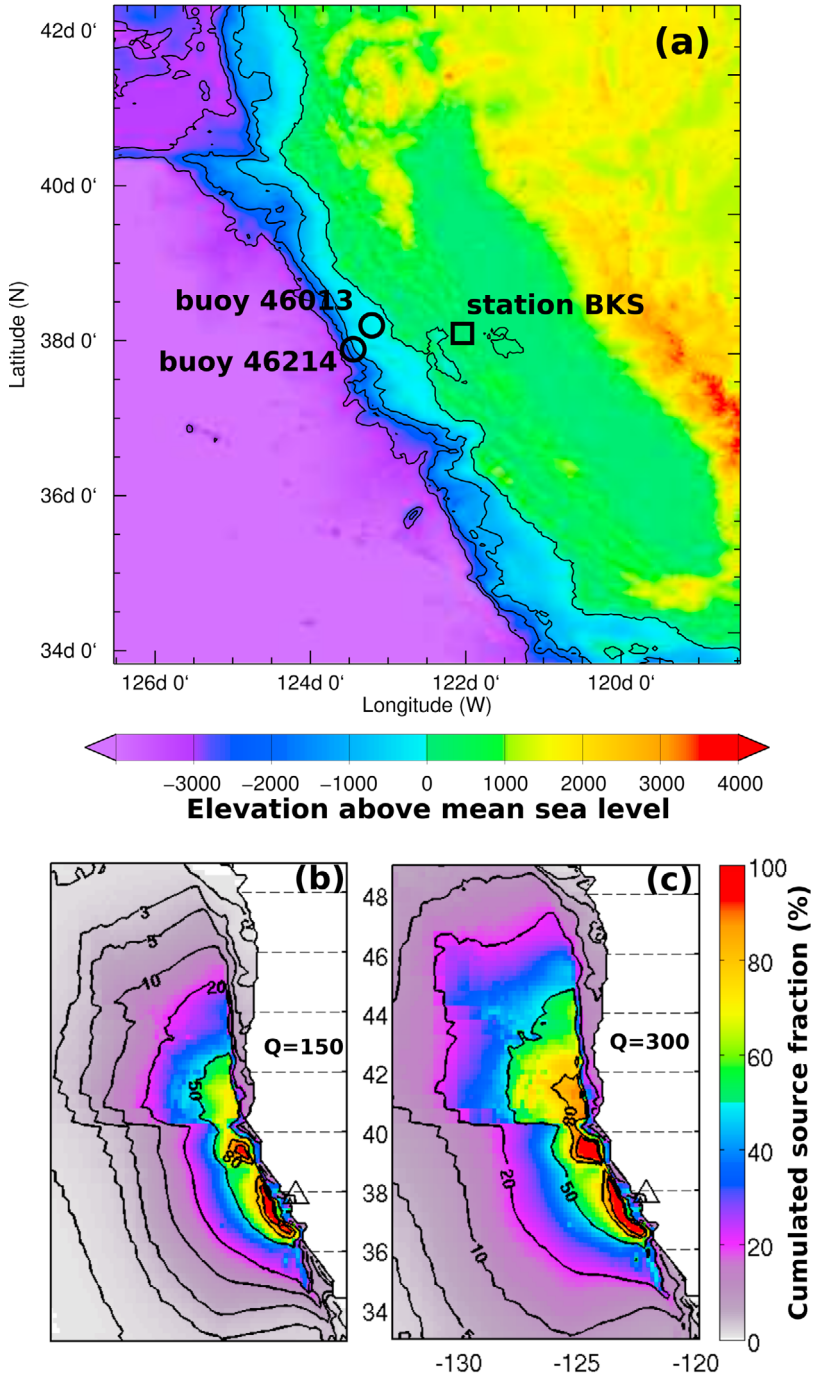

Figure 4. (a) Bathymetry and land topography of central California, and locations of wave buoys and Berkeley seismic station (BKS) whose data are analyzed here. (b and c) Maps of cumulated seismic source distribution for BKS, according to the ASSM model applied with two different values of the seismic damping Q. The color and contours give the percentage of the annual mean seismic energy at BKS which comes from outside any given contour. For example, only 20% of the ground displacement variance at BKS is caused by seismic sources outside of the 20% contour. The triangle is centered on BKS.

significant wave height estimated from the seismic spectrum is given by

$$H_{s,eq} = 4\sqrt{\int_{f_{\min}}^{f_{\max}} a(f)[F_\delta(f_s, t+\tau)]^{b(f)}\,\mathrm{d}f}. \qquad (13)$$

[40] When reconstructing the wave spectra and significant wave heights, as shown in Figure 6, a constant exponent $b = 0.5$ tends to give a limited range of values, with minima overestimated in summer and maxima underestimated in general. A frequency-dependent b appears better suited for

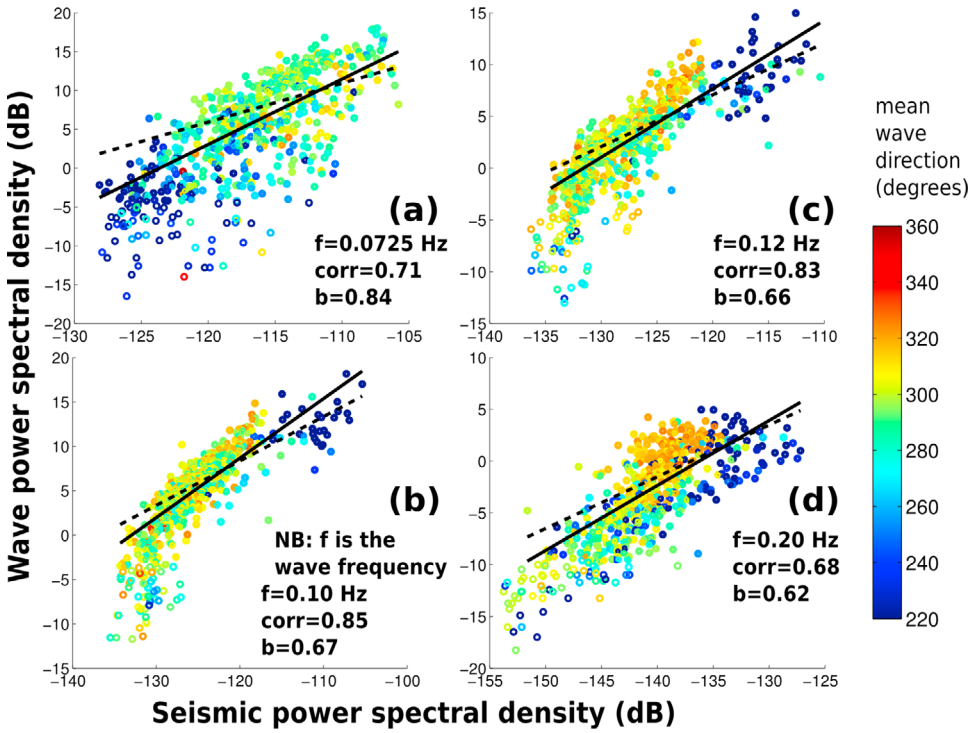

Figure 5. (a–d) Wave power spectral density $E(f)$ at buoy 46013 versus seismic displacement power spectral density $F_\delta(f_s)$ at BKS for four different ocean ave frequencies f, over January–April 2008, with one point every 4 hours and $f_s = 2f$. In each panel the dashed line is the best fit line (in linear scale) with a fixed exponent $b = 0.5$, and the solid line is the best fit line (in log scale) with a fitted exponent b. The colors indicate the mean wave direction at the buoy for the same frequency. The open symbols correspond to the lowest 10% wave spectral densities, which are not used in the fits. The ocean wave frequencies indicated on each panel are the central frequencies of the spectral bands, with a frequency increment of 0.005 Hz for $f < 0.1$ Hz and 0.01 Hz otherwise. The seismic spectra have been re-sampled with twice this ocean wave spectral resolution.

the reconstruction of extreme events. For example, on January 8, the estimated significant wave height (H_s) reaches 9.1 m, in close agreement with the observations.

[41] Table 1 gives error statistics for the reconstruction using various methodological refinements described below. The better quality of reconstructions with a frequency-dependent b is also demonstrated by the smaller errors on the mean periods, with a normalized root mean square error (NRMSE) of 10.4% instead of 12.4%. This smaller error shows that the spectral distribution of the energy is in better agreement with the observations.

3.3. Variability of Empirical Parameters With Noise Generation Classes

[42] A striking feature of our analysis is the seasonal variation of the exponent b in equation (12), as shown in Figure 7. We interpret this as a seasonal shift in the dominant class of noise generation, linked to seasonal patterns of winds and waves. This feature is robust because similar results are obtained when reconstructing data for the other buoy (number 46214), and the variation of b is stable for frequencies at which the correlation between spectral level time series is highest.

[43] ASSM analyzed that, in summer, dominant waves off this part of the coast are driven by along-shore winds, with a typical direction from 320°. This along-shore wind sea is hardly reflected by the shoreline and thus the directional integral $I(f)$ is simply given by the directional spectrum of a single wind sea in an unbounded ocean. Logically, the noise model of ASSM predicts that class I generation dominates in summers. This is illustrated by Figure 8, in which the thick green curve (modeled noise without reflection), follows very well the blue curve (observations) from May to mid-October. The fact that the green curve is almost on top of the red curve (full model including reflection) means that, according to the model, coastal reflection has no significant effect on the seismic noise sources. In contrast, during winter months, the wind and wave orientations yield stronger reflection at the coast, which makes class II the dominant noise generation pattern.

[44] Besides this seasonal variation, a few other outstanding events with high noise level are apparently not related to shoreline reflection but are instead strong class III generation events, which leads to an overestimation of the wave height (blue stars in Figure 8). For example, the erroneously high waves estimated on January 26 (blue star in Figure 6) correspond to a complex marine weather situation, with heavy swells opposing strong local wind-seas (Figure 14 in ASSM). The seismic root mean square displacement δ reached 2 μm, the second largest noise event in

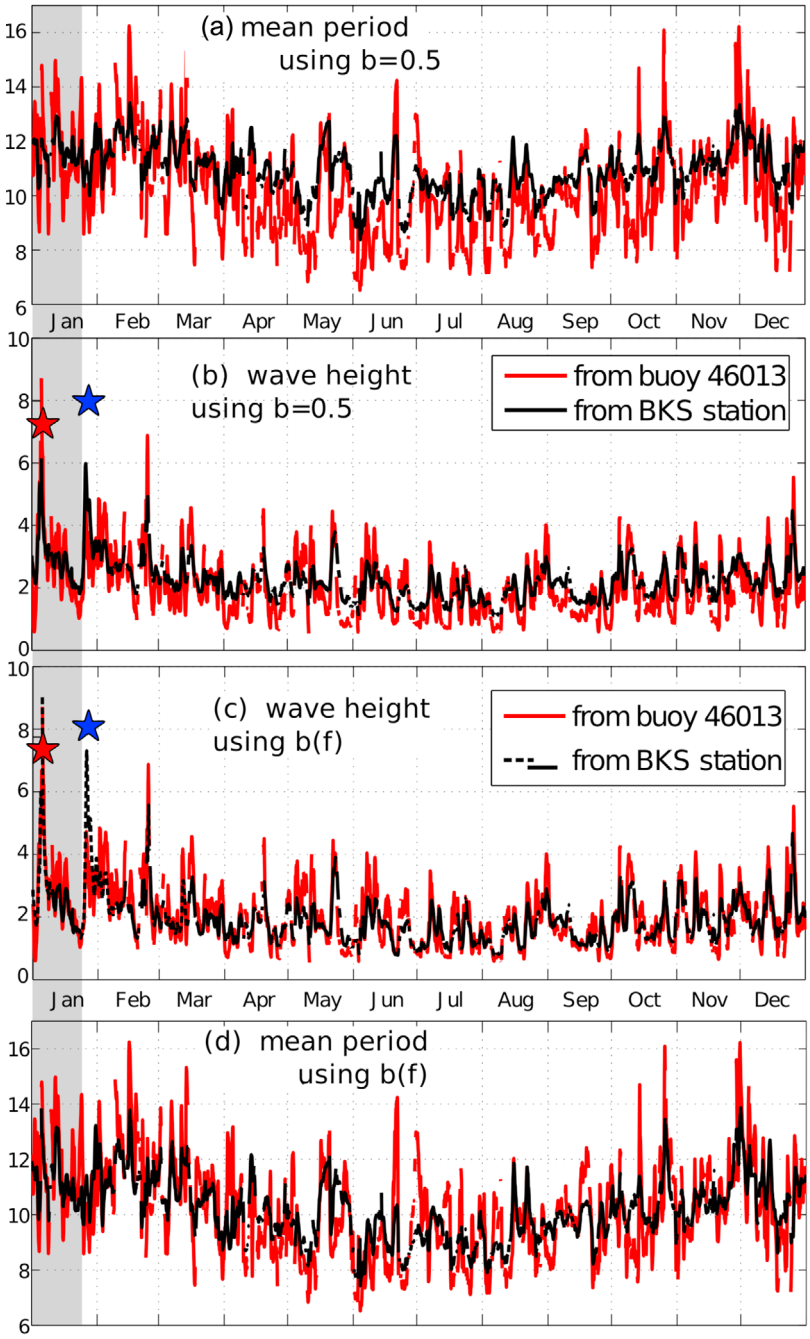

Figure 6. Measurements at buoy 46013 and estimations from the BKS seismometer of the mean period $T_{m0,-1}$ (Figures 6a and 6d), and the significant wave height (Figures 6b and 6c). The estimates use either (a and b) a fixed exponent b or (c and d) a frequency-dependent fitted exponent. In all cases the parameters a and b were fitted on the first 20 days of January only (shaded area). The red star marks a strong wave event on January 8, and the blue star marks a strong seismic noise event with limited wave height, on January 26, which is further analyzed in ASSM (their Figure 14), and due to class III generation with a swell interacting with the local wind sea. This analysis was corroborated by an examination of the COR seismic station in Oregon, that did not record any significant energy at the same frequency as BKS.

2008, although wave heights at buoy 46013 did not exceed 4.8 m, much less than the seismic estimate of 7.2 m (Figure 6) when using b (f) adjusted for the first 20 days of the year, or 10.1 m when b (f) is adjusted for the month of December. In this event, the noise model without reflection reproduces very well the observed seismic noise, which means that the effect of coastal reflection is negligible.

[45] The difference between class I and class II is less pronounced, but still the empirically fitted exponent b varies from 0.6 for class II to 0.9 for class I.

Table 1. Error Statistics for Wave Parameters at the Location of Buoy 46013 for the Year 2008 Using the BKS Seismic Data With Different Methods or the Global Numerical Wave Model of *Ardhuin et al.* [2010][a]

	H_s			$T_{m0,-1}$	
	NE (%)	r	NB (%)	NE (%)	r
BKS 2008 (dt = 4 h)					
b = 0.5 (20 days)	28.3	0.85	0.0	12.9	0.84
$b(f)$ (20 days)	25.1	0.85	−1.9	10.4	0.80
$b(f)$	25.7	0.85	0.0	10.0	0.84
$b(f)$, no class III	18.6	0.91	1.0	10.0	0.84
BKS 1994 (dt = 4 h)					
$b(f)$, no class III	20.8	0.83	0.4	8.6	0.83
BKS 2008 (daily)					
$b(f)$	22.4	0.87	0.1	9.0	0.87
$b(f)$, no class III	16.6	0.93	0.4	8.4	0.88
Model 2008 (dt = 3 h)	14.7	0.95	−3	9.1	0.93
Model 2004 (dt = 3 h)	14.9	0.94	−5	14.9	0.89
Model 1998 (dt = 3 h)	22.9	0.93	−15	10.5	0.91
Model 1994 (dt = 3 h)	13.6	0.93	−4.3	8.7	0.93

[a]Values are given for the following statistical parameters: the root mean square error normalized by the root mean square observed value (NE), Pearson's linear correlation (r), and the bias normalized by the r.m.s. observed value (NB). Correlations and r.m.s. errors are reduced when data are averaged for longer time steps dt, as illustrated here with 4 hours and 24 hours time steps. Several refinements are tested, from a constant b or variable $b(f)$ estimated on the first 20 days of the year, to separate estimations of $b(f)$ for winters and summers, with or without removing the class-III dominated events. For the years 2008 and 2004 the wave model is forced by operational analysis winds from the European Centre for Medium Range Weather Forecasting, for 1998, by the ERA40 re-analysis, and for the year 1994 by the Climate Forecast System Reanalysis [*Saha et al.*, 2010].

3.4. Wave Reconstruction Based on Noise Classification

[46] We now use our classification for improving the estimation of sea state parameters. The highest correlation between observed and estimated wave heights (r = 0.91 for 4-hourly values) is obtained when we eliminate class III events before estimating the exponent b, and do not include these events in the reconstruction of wave heights. For daily-mean values the correlation is as large as 0.93 with a normalized RMS error of 16.5%. For this, we have defined class III-dominated records as cases for which the noise model without reflection predicts a r.m.s. seismic displacement δ_{noref} larger than 0.5 μm at BKS, using U = 1.8km/s Q = 90, P = 1 (see equation 2). Similar results are obtained with Q = 300, P = 0.28 and the combination of the 0.16° and 0.5°-resolution models.

[47] With this definition, 3.6% of the time series are dominated by class III generation. In practice there is often some class II and class I generation from some regions of the ocean at the same time as class III in other regions. Yet this simple criterion serves our purpose of removing the largest outliers in a systematic way. This procedures does not remove weaker remote signals that may actually be due to any class of noise generation, such as the Atlantic storms recorded in Southern California and discussed by *Schulte-Pelkum et al.* [2004] and *Gerstoft and Tanimoto* [2007]. It would certainly be interesting to investigate possible systematic deviations associated with the presence of strong remote class II sources, in particular along the Oregon coast. This analysis is left for future studies.

[48] Based on our previous seasonal analysis we have assumed that class I dominates in summer (June to September) and class II dominates for other months. We thus take the averages of $a(f)$ and $b(f)$ for these two seasons, and apply either the winter or summer set of coefficients in equation (13). The difference between class I and class II is significant: if the same coefficients are applied for the entire year the correlation is limited, for the 4-hourly time series, to 0.89 with summer coefficients and 0.90 with winter coefficients (Figure 9).

[49] After calibrating our empirical model on the year 2008, we have applied it on other years, as illustrated on Figure 10 for the year 1994. In practice the buoy spectra for the year 1994 have a coarser frequency resolution and more limited frequency range, and the 2008 empirical model was estimated on similarly coarsened 2008 data. The year 1994 is particular with a low level of long period swells, resulting in shorter mean periods, and much more frequent significant sources of noise that, according to the ASSM model, are not related to coastal reflection. Yet the empirical model for 2008 reproduces well the observed wave heights on average. The definition of class III ($\delta_{\mathrm{noref}} > 0.5$ μm) still leaves too many outliers that are effectively removed by redefining class III as $\delta_{\mathrm{noref}} > 0.1$ μm, but then a large fraction of the time series is lost.

[50] This example suggests that the retrieval of extreme wave statistics from seismic noise will likely require other techniques, such as proposed by *Ebeling and Stein* [2011] for Hurricanes, but it suggests that the average sea state can be well reproduced by our simple method.

[51] In summary, it is possible to reconstruct wave parameter time series with random errors that are comparable to those of uncalibrated numerical wave models forced by re-analysis winds (Table 1). More interestingly, the wave parameters have more stable and smaller biases, compared to uncalibrated numerical wave models.

4. Seismic Noise From Strong Remote Sources

[52] Sea state estimation is more complex when seismic stations record noise from a large part of an ocean basin. First of all, no single wave buoy is representative of the sea states that contribute to the recorded seismic noise, so that it is not simple to define wave observations for calibration. Secondly, the sources may be generated by a much wider range of sea states, including many class III events, so that empirical seismic-ocean wave relationship can be less robust. Still, the recorded seismic level may be linked with some measure of the wave energy over the area of noise generation.

[53] We take two examples, one from the North Pacific and another from the North Atlantic.

4.1. Wave Heights From Noise Recorded at Kipapa (KIP, Oahu, Hawaii)

[54] Based on the ASSM model, a disk with radius 1000 km around KIP is expected to contain only half the sources seen by the station. This model was verified using higher resolution grids, down to 500 m along the shoreline with a finite element mesh similar to the one used by *Ardhuin et al.* [2009a]. The model underestimates the seismic noise level for f_s < 0.16 Hz, probably due to an

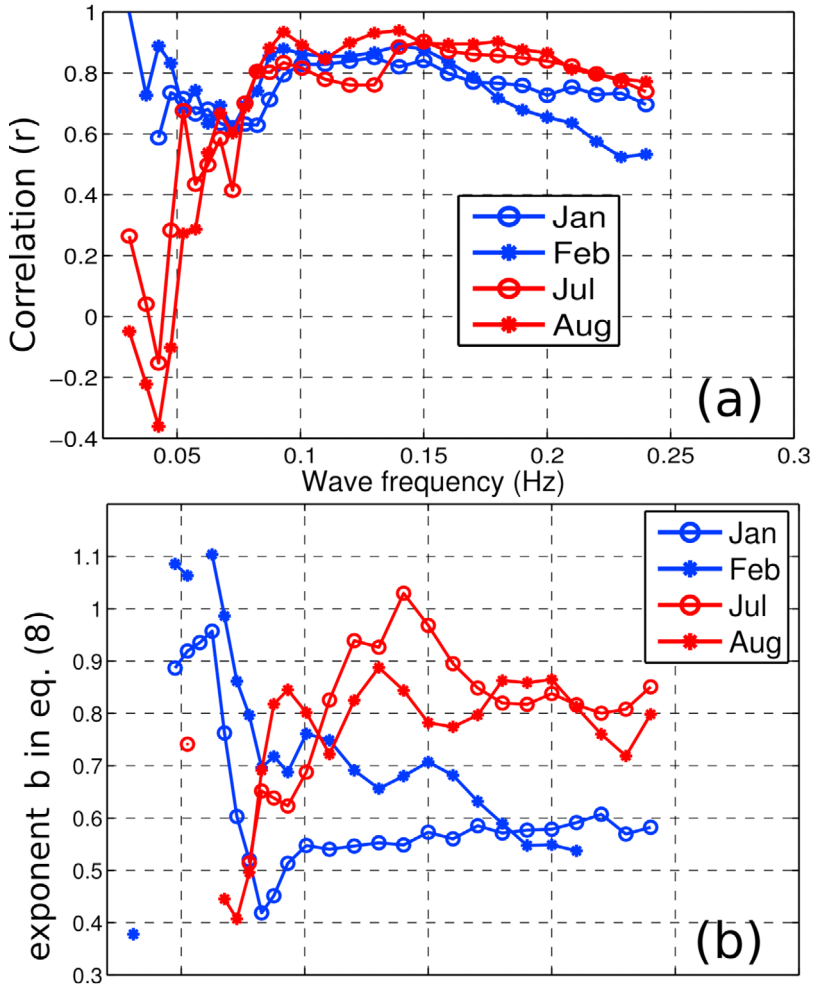

Figure 7. (a) Correlation of $E(f, t)$ and $F_\delta(f_s, t + \tau)$ for $\tau = 2$ hours and $f_s = 2f$ for selected winter (blue) and summer (red) months. (b) Exponent b in equation (12) as a function of frequency for the months of January, February, July and August of 2008. Values of b are only shown for significant correlations ($r > 0.5$). The low frequencies ($f < 0.05$), in particular in summer, are contaminated by other noise generation mechanisms.

underestimation of coastal reflections by a constant coefficient. In order to test the relationship between wave heights and seismic noise, we use satellite altimeter data. These data are very sparse is time, but in the 50% source region and for the year 2008, there is at least one pass every day by one of the three satellites, Jason-1, Envisat, and Geosat-Follow-On.

[55] Starting from the source of seismic noise given by equation (5), we integrate over the dominant noise frequency band,

$$S_{DF,I}(\lambda, \phi, t) = \int_{0.08\mathrm{Hz}}^{0.32\mathrm{Hz}} S_{DF}(\lambda, \phi, f_s, t)\mathrm{d}f_s. \qquad (14)$$

This time-dependent integrated noise source is then used to define constant weights

$$w(\lambda, \phi) = \sum_{i=1}^{N} \frac{S_{DF,I}(\lambda, \phi, i)}{H_s^2(\lambda, \phi, i)}, \qquad (15)$$

where i is a time index, and N are the number of time steps. Here we sum over the entire year so that $N = 2190$.

[56] Using these time-independent weights, we now obtain an estimate of the daily averaged wave height

$$\langle H_s \rangle = \sqrt{\frac{\sum w(\lambda, \phi) H_s^2(\lambda, \phi)}{\sum w(\lambda, \phi)}}. \qquad (16)$$

We find that $\langle H_s \rangle$ is highly correlated with the daily mean recorded seismic displacement $\langle \delta_{\mathrm{rms}} \rangle$ (Figure 11b). A good estimator of North Pacific wave heights is

$$\langle H_s \rangle \simeq 1.4\mathrm{m} + 0.64 \times 10^6 \langle \delta_{\mathrm{rms}}(\mathrm{KIP}) \rangle. \qquad (17)$$

The large 1.4 m offset in equation (17) is likely related to the high level of background swell energy that, by itself, has only a small contribution to the noise through the reflection at the shorelines. The otherwise linear relationship may be a bit surprising given that the analysis of noise events for KIP shows that many large noise events belong to class III with the interaction of two independent wave systems (e.g., Figure 11 of ASSM). Although a higher sea state generally gives a higher seismic noise, this is only true if the

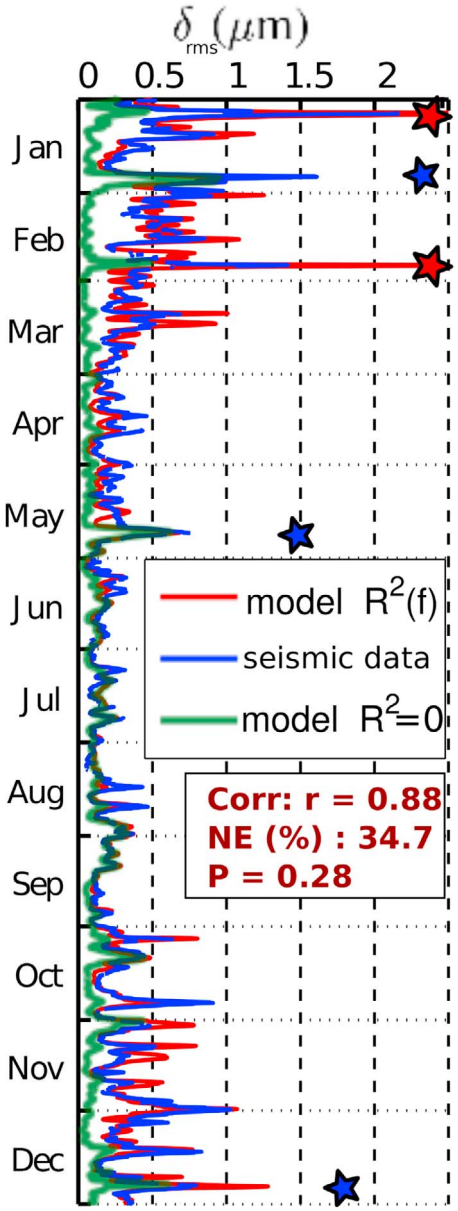

Figure 8. Observed and modeled RMS vertical seismic displacement at BKS, for the year 2008. The model is based on equation (2) with Q = 300 and P = 0.28. The statistics given quantify the model-observation differences, with NE and r defined in Table 1. The blue stars mark large class III events, including January 26. The two red stars correspond to situations where the model with a linear reflection largely over-predicts the observed levels, with δ_{rms} estimated as high as 7.5 μm. These overestimations correspond to the two strongest storms of 2008, with ocean wave heights of 9.5 and 7 m measured by the 46013 buoy, while heights are less that 6 m for the rest of the year. In such cases our shoreline reflection coefficient $R^2(f)$ is overestimated [*Elgar et al.*, 1994; *O'Reilly et al.*, 1999].

directional properties of ocean waves do not vary too strongly. This variation of the directional properties is the likely cause of the scatter between recorded noise and average wave heights.

[57] Replacing the satellite-derived wave heights by the results of the numerical wave model of *Ardhuin et al.* [2010], with a spatial resolution of 0.5 degree in longitude and latitude and a time step of three hours, we find that the full space-time coverage of the model produces only a marginally better correlation with the seismic noise (Figure 12b). From this we

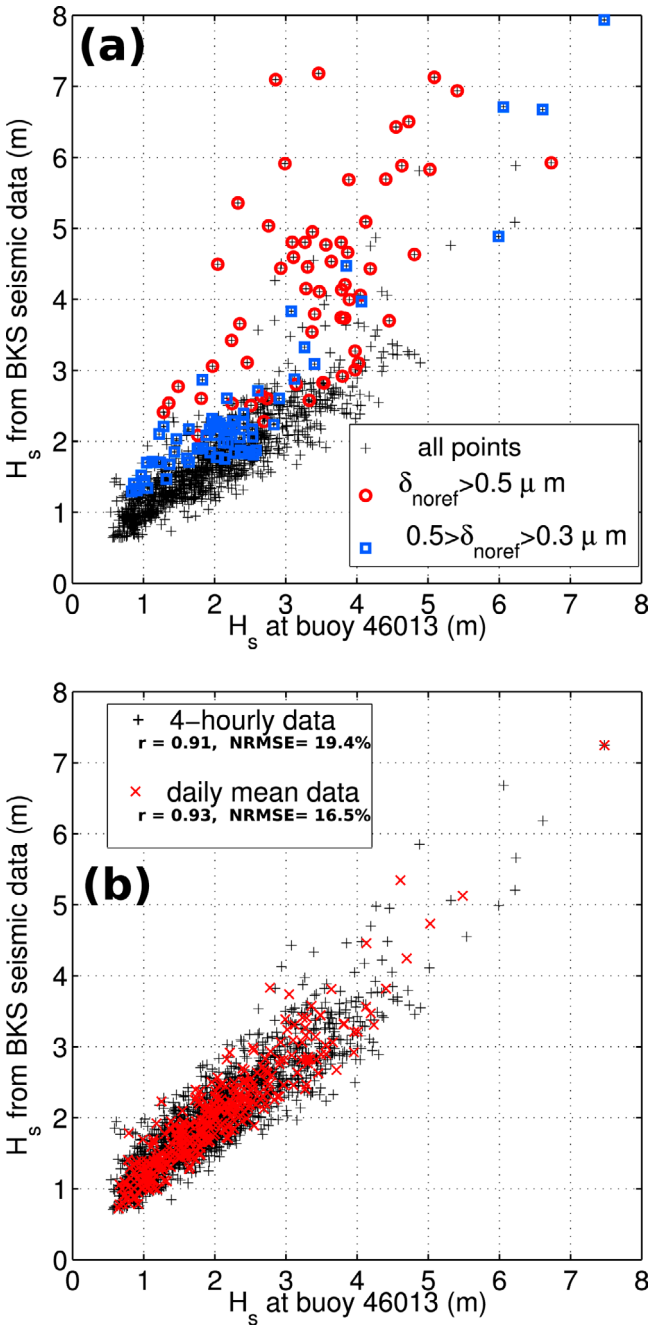

Figure 9. Wave height inferred from the seismic displacement at BKS versus the wave height measured by the buoy 46013 when using different coefficients $a(f)$ and $b(f)$ for winter and summer months. (a) $H_{s,eq}$ is estimated using equation (13) with $a(f)$ and $b(f)$ defined from the full time series, (b) $a(f)$ and $b(f)$ are estimated after removing potential class III event, defined by $\delta_{noref} > 0.5$ μm.

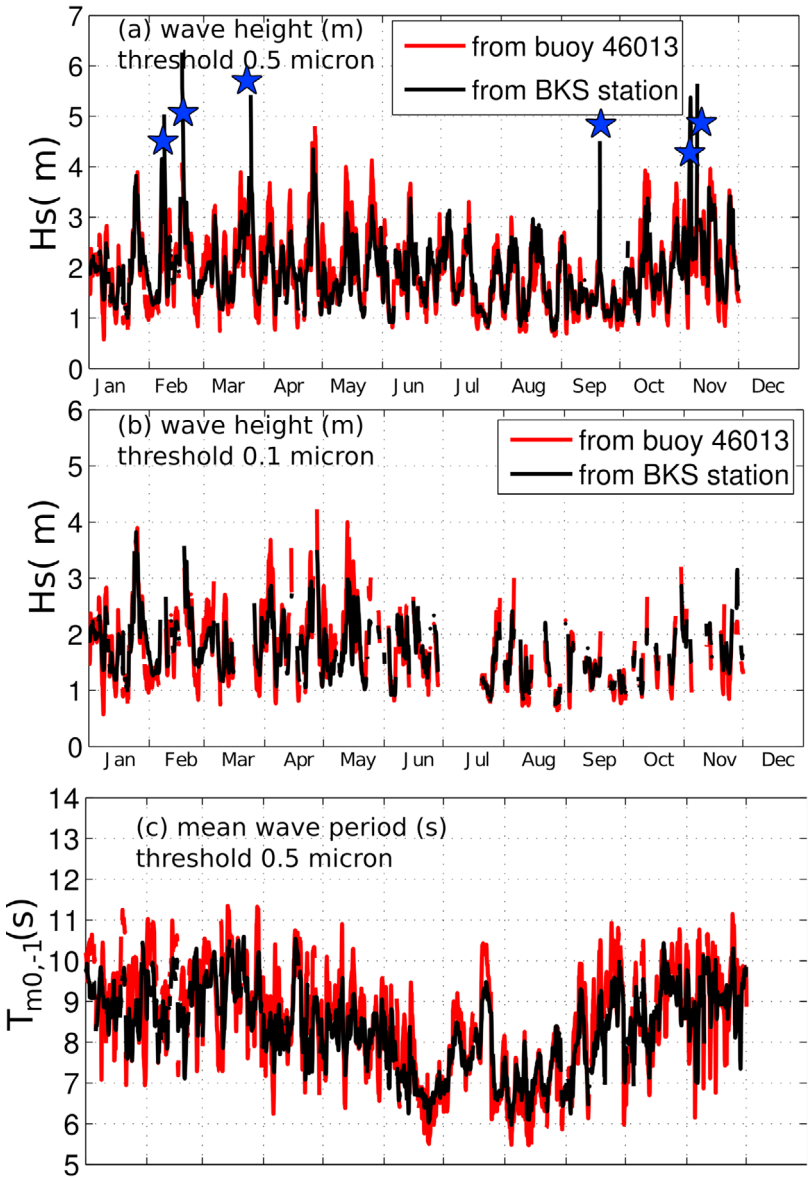

Figure 10. Same as Figures 6c and 6d for the year 1994. The wave parameters estimated from the BKS seismometer are based on the empirical model fitted for the year 2008. (a) We use the same threshold as in 2008 to define class III events, and (b) this threshold is reduced to 0.1 microns.

conclude that the uncertainty in the estimation of sea state parameters is real, and not an artifact of the limited sampling of the satellite data used for validation.

4.2. Wave Heights From Noise Recorded at Eskdalemuir (ESK, Scotland)

[58] In the North Atlantic, there is also ample evidence for a correlation of sea states and seismic noise [*Essen et al.*, 1999, 2003], but this has usually been investigated by correlating time series of one seismic station with wave data from a single point. Here we use an area-averaged wave height based, again, on the expected spatial distribution of seismic sources from the ASSM model (Figure 13a), and we analyze the seismic record of the ESK station. Because we expect that the noise sources for ESK have a smaller spatial extension than for KIP, the altimeter sampling error becomes more important and we prefer to compare modeled wave heights with noise energy levels. The correlation between modeled wave heights and the seismic RMS displacement at ESK is $r = 0.84$, compared to 0.81 using altimeter data (Figure 13b). The daily mean wave height thus explain at least $r^2 = 70\%$ of the variance in seismic noise amplitude at ESK.

[59] However, recorded RMS ground displacements are more tightly correlated with modeled noise using the ASSM model with a seismic wave damping factor $Q = 300$, Rayleigh group velocity $U = 1.8$km/s, and propagation factor $P = 0.842$. For a smaller time step of 3 hours the correlation is already as high as 0.95 as shown on Figure 13c. This difference between 0.84 and 0.95 must be due to the

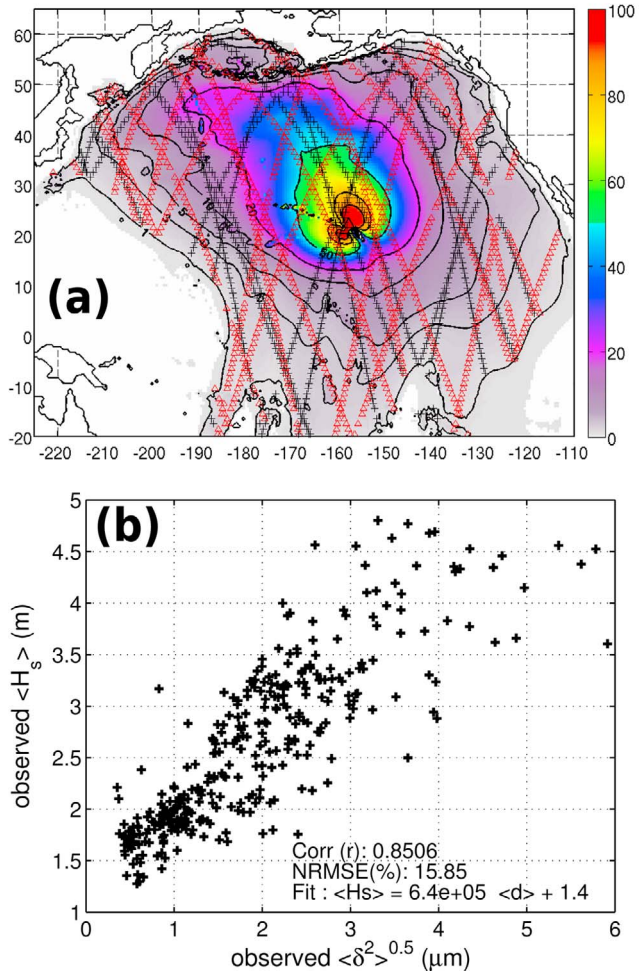

Figure 11. (a) Same as Figure 4 but for the Kipapa (KIP) station, with superimposed satellite tracks for January 1 2008 (black crosses) and January 2 2008 (red triangles). (b) Observed daily mean wave height in the North Pacific in 2008 from JASON, ENVISAT and GFO satellite altimeters, weighted according the ASSM model of seismic source distribution using Q = 700, against the daily mean standard deviation of vertical ground motion at KIP.

variability in the directional wave distributions that change the values of $I(f)$ so that the same wave energy can give very different seismic noise levels. At any given time, the noise comes from a limited area within all the possible source locations seen over the year. The possible interpretation of the noise as an area average is thus misleading.

[60] Understanding and possibly parameterizing the variability of $I(f)$ will thus be needed to arrive at more accurate sea state estimations from seismic noise. This may be achieved by a seismic array analysis, as performed by *Haubrich and McCamy* [1969], which provides a time-varying spatial distribution of the field of noise sources.

5. Summary and Perspectives

[61] Previous empirical estimation methods for deriving ocean wave parameters from seismic noise were based on *a priori* relationships between wave and seismic noise spectra. Using a numerical model for seismic noise we were able to show that the wave to noise transfer function is generally complex, due to the role of the directional distribution of wave energy.

[62] Our first conclusion is that it is paramount to have a basic knowledge of the spatial distribution of the noise sources that contribute to the record at a given seismic station. This is where the direct numerical noise model is most useful. Some stations, most notably in Hawaii, record noise that was probably generated in a large portion of an ocean basin, while others only record noise mostly generated over a nearby ocean area. The most common situation is intermediate, as we have found for many stations on mid-oceanic islands.

[63] In the case where the seismic station record is dominated by local sources, it is relatively simple to correlate the seismic spectra with data from one representative point in

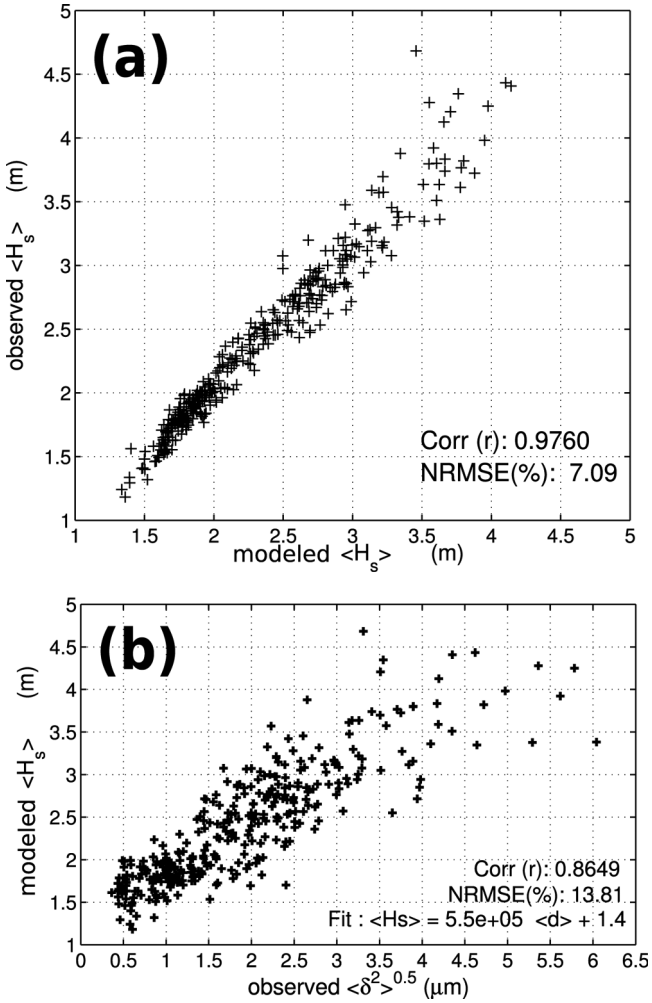

Figure 12. (a) Correspondence between daily averages of modeled and satellite-derived wave heights. (b) Modeled daily mean wave height in the North Pacific in 2008, using the global 0.5° resolution model of *Ardhuin et al.* [2010] and weighted according to the ASSM model, against the daily mean standard deviation of vertical ground motion at KIP.

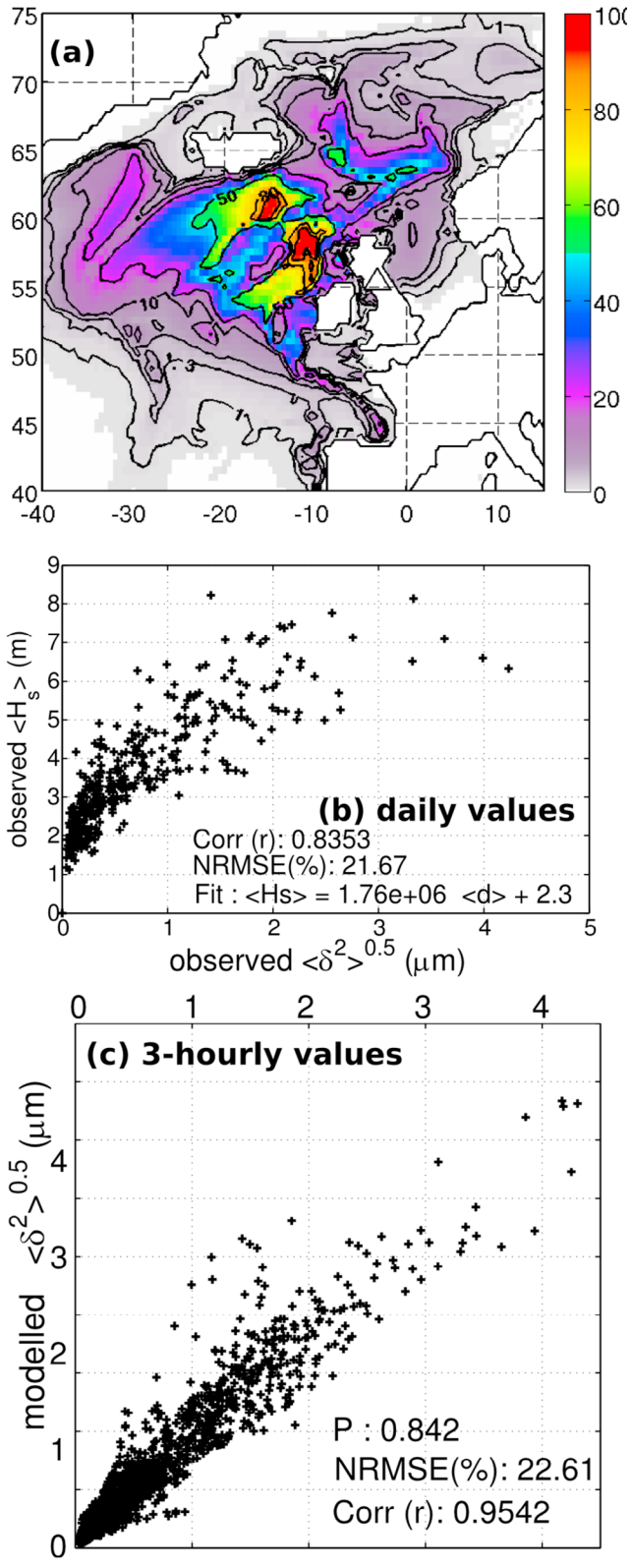

Figure 13. (a) Same as Figure 4 but for the Eskdalemuir (ESK, Scotland) station. (b) Modeled daily mean wave height in the North-East Atlantic in 2008, weighted according to the ASSM model of seismic source distribution, against the daily mean standard deviation of vertical ground motion at ESK. (c) Modeled against observed seismic displacement at ESK every 3 hours.

the ocean, and two main situations emerge which can lead to simplified and invertible transfer functions for noise generation dominated by classes I and II.

[64] When the presence of opposite wave directions is due to coastal reflection, as considered by *Zopf et al.* [1976] and *Bromirski et al.* [1999], noise level at any frequency is well correlated with the wave spectral density at half that frequency, to an exponent $b \simeq 0.7$. The departure of this exponent from 0.5 is due to the general decrease of reflection coefficients when wave energy increases. In some particular settings when dominant winds blow alongshore, such as off Central California in summers, wave reflection has little to do with noise generation. Noise then apparently results from the broad directional distribution of the wind-sea, which contains enough energy in opposing directions to explain the observed seismic noise. In this case, the noise spectrum is almost proportional ($b \simeq 0.9$) to the wave spectrum at half the seismic frequency, which means that the directional integral I in the noise generation varies almost like the inverse of the wave energy. In the case of Central California, these two situations are typical of winters and summers, respectively, and a numerical noise model, or some information on wind direction can be used to make a fine discrimination between the two cases.

[65] Some kind of noise model will be most relevant for finding, in the noise record, the third class of noise generation, that provides intense noise level when two independent wave systems with opposing directions and same frequency coexist. These events can lead to strong overestimations of wave heights. Once they are removed, the correlation between measured daily mean wave heights and estimates from the seismic station can be as high as 0.93. These improvements in the wave reconstruction can be applied to investigate past wave climates more accurately. Yet, the investigation of extreme events should be considered with caution due to possible class III contamination.

[66] For seismic stations that appear to be representative of a large oceanic area, due to a weaker seismic attenuation or a wider spatial distribution of sources, data from a single seismic station can be related to an area-averaged wave height. This is the case of North-Western European stations and all the oceanic island stations that we have investigated (in Azores, Falkland Islands, Martinique, Reunion, Easter Island, French Polynesia). For these, the larger variability of wave directional properties across the source area results in a relatively larger scatter. Estimated wave heights are correlated with observed or modeled wave heights, but linear correlation coefficients are typically less than 0.88 for daily mean values. For all seismic stations, we expect that seismic-derived wave heights averaged over time periods of one month or one year, or results of direct seismic modeling, as done by ASSM, can be useful datasets for correcting the slow drift of numerical wave models.

Appendix A: Seismic Sources of Class I, From a Single Wind Sea

[67] This situations occurs everywhere in the ocean, but generally produces only a low level of noise at periods 4 to 6 s, and it probably dominates at periods shorter than 1 s. The wind sea amplified by the local wind fills the high frequency part of the wave spectrum and generally co-exists

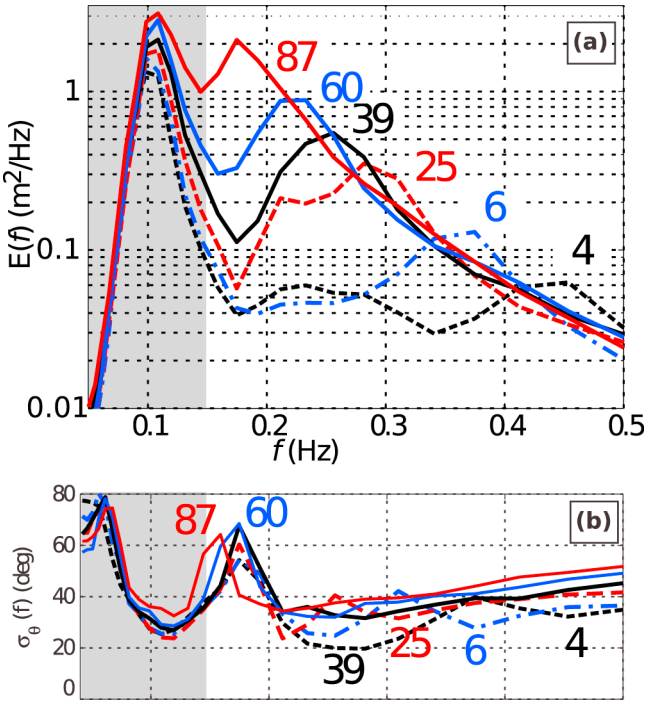

Figure A1. Example of evolution of (a) the spectral wave density $E(f)$ with fetch, and (b) directional spreading $\sigma_1(f)$. Each curve corresponds to a different location with the fetch indicated by the numbers (in kilometers). These are observed spectra and spreads averaged over 6 hours during one event on 3 November 1999, during the Shoaling Waves Experiment [adapted from *Ardhuin et al.*, 2007]. The shaded gray frequency range corresponds to swells from the open ocean, while the higher frequencies are wind-sea waves generated by an offshore wind of 9.5 m/s.

with swell energy at lower frequencies. The interaction of swell and wind sea will not produce any noise if their frequency range does not overlap. This is the case for the wave spectra shown in Figure A1. In order to understand the relationship between the wave spectrum and the seismic spectrum, proportional to $E^2(f)I(f)$ according to theory, one should consider the evolution of the directional properties of the wind-sea waves, and hence the $I(f)$ term, together with the variation in the spectral density $E(f)$. When a single wave system is present, the spectral shape should vary smoothly as a function of wave age [*Long and Resio*, 2007] and we expect that $I(f)$ increases with the directional spreading, as defined by equation (7).

[68] Considering waves generated by the local wind, the directional spreading is minimum at the peak frequency and increases both for higher and lower frequencies, where the spectral density E is lower [e.g., *Hasselmann et al.*, 1980] (see also Figure A1). As a result, there is a strong anti-correlation between $E(f)$ and $\sigma_1(f)$, in particular for intermediate frequencies. Figure A2 shows examples of this anti-correlation with summer waves recorded by the Datawell Waverider buoy operated by the Coastal Data Information Program (CDIP), offshore of Point Reyes, California. Because we expect $I(f)$ to vary with σ_1, there should also be an anti-correlation of $I(f)$ with $E(f)$.

[69] For a wavefield that varies on scales much larger than the seismic attenuation scale $UQ/(2\pi f_s)$, we may take the wave parameters $E(f)$ and $I(f)$ outside of the integral (2),

$$F_\delta(\lambda,\phi,f_s) \simeq \frac{2\pi f_s^2 \tilde{C} \rho_w^2 g^2 E^2(f) I(f)}{\rho_s^2 \beta^5 R_E} \int_\Omega \frac{\mathrm{e}^{-2\pi f_s R_E \Delta/(UQ)}}{\sin\Delta} \mathrm{d}A. \quad \text{(A1)}$$

The integral in equation (A1) does not depend on the wave energy anymore.

Appendix B: Seismic Sources of Class II, With Coastal Reflection

[70] We define the reference wave direction to be in the shore-normal direction $\theta_n = 0$. We also split the directional distribution in incident and reflected components,

$$M(f,\theta) = M_i(f,\theta) \text{ if } -\pi/2 < \theta < \pi/2 \quad \text{and} \quad \text{(B1)}$$

$$M(f,\theta) = M_r(f,\theta) \text{ otherwise.} \quad \text{(B2)}$$

The full directional spectrum is still normalized as usual, and we split the directional distribution in incident and reflected components,

$$\int_0^{2\pi} M(f,\theta)\mathrm{d}\theta = \int_{-\pi/2}^{\pi/2} M_i(f,\theta)\mathrm{d}\theta + \int_{\pi/2}^{3\pi/2} M_r(f,\theta)\mathrm{d}\theta = 1. \quad \text{(B3)}$$

[71] If reflection were a linear process, for any incident component of direction θ' with a directional spectral density

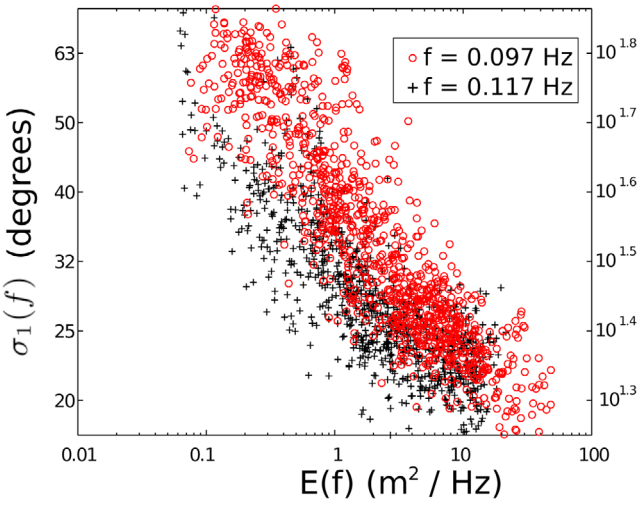

Figure A2. Correlation between the directional spread $\sigma_1(f)$ and the spectral density $E(f)$ for June to September months of 2008 at the Point Reyes CDIP buoy (WMO number 46214). Each symbol corresponds to one 3-hour record. Spectral data was averaged around two central frequencies, 0.097 and 0.117 Hz, that are representative of the general behavior of the wind seas observed in summer, with a bandwidth of 0.009 and 0.011 Hz, respectively.

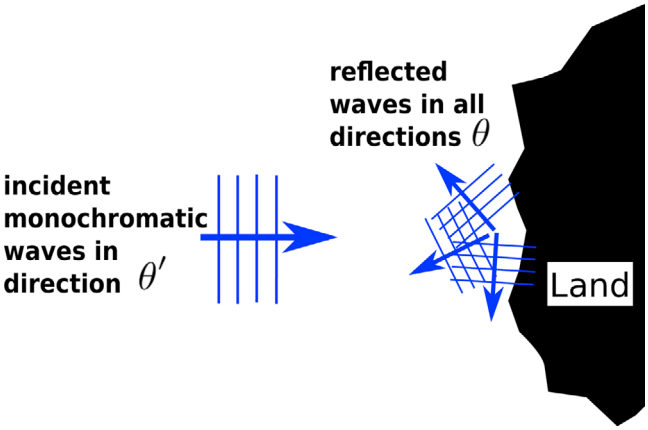

Figure B1. Illustration of the directionally-spread waves reflected from an incident monochromatic wave train.

$M_i(f, \theta')$ we get waves in the reflected direction θ, as shown in Figure B1, with a directional distribution

$$N_r(f, \theta', \theta) = R_s^2(f, \theta', \theta) M_i(f, \theta'), \tag{B4}$$

where $R_s^2(f, \theta', \theta)$ is a reflection coefficient for the energy scattered in direction θ, so that the usual energy reflection coefficient, energy ratio of all reflected waves and their associated monochromatic incident wave train, is

$$R^2(f, \theta') = \int_{\pi/2}^{3\pi/2} R_s^2(f, \theta', \theta) \mathrm{d}\theta. \tag{B5}$$

The above integral spans the reflected directions $\pi/2$ to $3\pi/2$ since we have defined $\theta' = 0$ as the direction of the normally incident waves.

[72] The exact definition of R_s depends on where exactly (equation B4) is evaluated because most of the reflected waves, with energy $E(f)M_r$, turn back toward the shore due to refraction, and the incident waves, with energy $E(f)M_i$, are dissipated by breaking in the surf zone. Thus both the incident and reflected wave energy vary rapidly in the cross-shore direction, and so does their ratio which defines the reflection coefficient. We consider that R_s is defined from wave spectra just outside of the surf zone. The reflected waves decay away from the reflector due to refraction, but also damping by air-sea interactions, which typically occurs over scales of the order of 100 to 1000 km for dominant oceanic waves [*Ardhuin et al.*, 2009a]. Within this distance from the reflector, the full directional spectrum thus contains the incident and reflected waves,

$$M(f, \theta) = M_i(f, \theta) + \int_{-\pi/2}^{\pi/2} R_s^2(f, \theta', \theta) M_i(f, \theta') \mathrm{d}\theta', \tag{B6}$$

with $-\pi/2 < \theta < \pi/2$ for the first (incident) term and $\pi/2 < \theta < 3\pi/2$ for the second (reflected) term. In the second term the incident directions θ' that give rise to a reflection in direction θ naturally span the range of incident directions, i.e. $-\pi/2$ to $\pi/2$. The directional integral thus becomes

$$I(f) = \int_{-\pi/2}^{\pi/2} M_i(f, \theta) \int_{-\pi/2}^{\pi/2} M_i(f, \theta') R_s^2(f, \theta', \theta + \pi) \mathrm{d}\theta' \mathrm{d}\theta. \tag{B7}$$

[73] In general $R^2 < 0.1$, and we may neglect the reflected contribution in equation (B3), which gives $\int_{-\pi/2}^{\pi/2} M_i(f, \theta) \simeq 1$. We now consider a narrow incident spectrum with a mean direction θ_m, such that $M_i(f, \theta) \simeq \delta(\theta - \theta_m)$. Defining the reflection direction for the opposite direction $R_o^2(f, \theta_m) = R_s^2(f, \theta_m, \theta_m + \pi)$, the integral (B7) becomes,

$$I(f) \simeq R_o^2(f, \theta_m). \tag{B8}$$

Appendix C: Homogeneity of Sea States in the Source Region

[74] For all classes it is most important to consider the spatial extent of the source area. Indeed the expected relationship for classes I and II can be put in the form given by equation (12) provided that seismic sources are distributed within an area of the order of, or smaller than, the correlation scales of the wavefield, which range from about 300 km for wind-seas to 1000 km or more for swells [*Queffeulou*, 1983; *Delpey et al.*, 2010]. Otherwise, the wave spectrum estimated with equation (12) may be interpreted as a spatial average, and will not correlate well with a point measurement such as given by a buoy.

[75] For class II, there is a natural spatial scale imposed by the area of overlap of the incident and reflected wave trains, where incident waves can oppose the waves reflected from other incident waves that have traveled ahead. Severe storms that generate very long waves generally have a 6 to 12 hour peak power and a core that is well defined spatially, where most of the long wave energy is generated [e.g., *Delpey et al.*, 2010]. On Figure 2, if the storm S1 is very far from land, the swell travel time from S1 to B can be much larger than the storm duration. In this case there will only be a significant seismic source at B if waves from the nearside of the storm (point A in Figure 2) have the time to reflect off the shore and travel back to B to meet waves from the far side of the storm (point D in Figure 2). Thus the distance X from the shore is typically less than half the storm diameter D_S. For moving storms with continuous wave generation, X can be larger. Because it takes bigger storms to generate waves with longer periods, the ASSM model predicts significant seismic noise generation over distance from shore that ranges from 300 km to 1000 km for the longest wave periods. At these scales, the dissipation of swells is generally negligible [*Ardhuin et al.*, 2009b].

[76] Yet, given the seismic wave attenuation factor UQ, which depends on the Earth's crust properties, these distances can be much larger than the area from which seismic waves can actually be recorded. Taking $U = 1.8$ km s^{-1}, with a factor $Q = 100$, seismic energy at $f_s = 0.15$ Hz is halved every 120 km of propagation (Figure 1a). Also, significant noise generation only occurs for water depths larger than a few hundred meters. As a result, the generation area seen by the seismic station is often limited to a narrow strip near the shelf edge (e.g., Figure 4). In these conditions, there may be only a limited spatial variability of the wave frequency spectrum $E(f)$ and directional properties, except for the possible existence of offshore islands or headlands and steep submarine topography [e.g., *Pawka*, 1983; *Magne et al.*, 2007].

[77] **Acknowledgments.** We thank the operators of GEOSCOPE, Berkeley Digital Seismic Network, and IRIS/IDA for providing excellent broadband seismic data. Data were taken from both GEOSCOPE and IRIS data centers. Wave data were provided by the U.S. National Data Buoy Center and the Coastal Data Information Program. F.A. and A.B. are funded by ERC grant 240009 "IOWAGA" with additional support for F.A. from the U.S. National Ocean Partnership Program, under grant N00014-10-1-0383, and the Centre National d'Etudes Spatiales (CNES). The paper uses observations with altimeters embarked on Jason-1, Envisat and ERS-2. The manuscript was greatly improved thanks to the remarks of two anonymous reviewers.

References

Algué, J. (1900), Relation entre quelques mouvements microséismiques et l'existence, la position et la distance des cyclones à Manille (Philippines), in *Congrès international de Météorlogie, Paris*, pp. 131–136, Gauthier-Villars, Paris.

Ardhuin, F., and R. Magne (2007), Current effects on scattering of surface gravity waves by bottom topography, *J. Fluid Mech.*, *576*, 235–264.

Ardhuin, F., T. H. C. Herbers, K. P. Watts, G. P. van Vledder, R. Jensen, and H. Graber (2007), Swell and slanting fetch effects on wind wave growth, *J. Phys. Oceanogr.*, *37*(4), 908–931, doi:10.1175/JPO3039.1.

Ardhuin, F., L. Marié, N. Rascle, P. Forget, and A. Roland (2009a), Observation and estimation of Lagrangian, Stokes and Eulerian currents induced by wind and waves at the sea surface, *J. Phys. Oceanogr.*, *39*(11), 2820–2838.

Ardhuin, F., B. Chapron, and F. Collard (2009b), Observation of swell dissipation across oceans, *Geophys. Res. Lett.*, *36*, L06607, doi:10.1029/2008GL037030.

Ardhuin, F., et al. (2010), Semi-empirical dissipation source functions for wind-wave models: Part I, definition, calibration and validation, *J. Phys. Oceanogr.*, *40*(9), 1917–1941.

Ardhuin, F., E. Stutzmann, M. Schimmel, and A. Mangeney (2011a), Ocean wave sources of seismic noise, *J. Geophys. Res.*, *116*, C09004, doi:10.1029/2011JC006952.

Ardhuin, F., J. Tournadre, P. Queffelou, and F. Girard-Ardhuin (2011b), Observation and parameterization of small icebergs: Drifting breakwaters in the southern ocean, *Ocean Modell.*, *39*, 405–410, doi:10.1016/j.ocemod.2011.03.004.

Aster, R. C., D. E. McNamara, and P. D. Bromirski (2010), Global trends in extremal microseism intensity, *Geophys. Res. Lett.*, *37*, L14303, doi:10.1029/2010GL043472.

Barruol, G., D. Reymond, F. R. Fontaine, O. Hyvernaud, V. Maurer, and K. Maamaatuaiahutapu (2006), Characterizing swells in the southern pacific from seismic and infrasonic noise analyses, *Geophys. J. Int.*, *164*, 516–542, doi:10.1111/j.1365-246X.2006.02871.x.

Bernard, P. (1937), Relation entre la houle sur la côte nord du Maroc et l'agitation microséismique en Europe occidentale, *C. R. Acad. Sci. Paris*, *205*, 163–165.

Bernard, P. (1941), Sur certaines proprietes de la boule etudiées a l'aide des enregistrements seismographiques, *Bull. Inst. Oceanogr. Monaco*, *800*, 1–19.

Bernard, P. (1981), Sur l'existence et l'amplitude de la variation undécennale des microséismes météorologiques, *C. R. Acad. Sci. Paris*, *293*, 687–689.

Bernard, P. (1990), Historical sketch of microseisms from past to future, *Phys. Earth Planet. Inter.*, *63*, 145–150.

Bromirski, P. D., and F. K. Duennebier (2002), The near-coastal microseism spectrum: Spatial and temporal wave climate relationships, *J. Geophys. Res.*, *107*(B8), 2166, doi:10.1029/2001JB000265.

Bromirski, P. D., R. E. Flick, and N. Graham (1999), Ocean wave height determined from inland seismometer data: Implications for investigating wave climate changes in the NE Pacific, *J. Geophys. Res.*, *104*(C9), 20,753–20,766.

Bromirski, P. D., F. K. Duennebier, and R. A. Stephen (2005), Mid-ocean microseisms, *Geochem. Geophys. Geosyst.*, *6*, Q04009, doi:10.1029/2004GC000768.

Caires, S., and A. Sterl (2005), 100-year return value estimates for ocean wind speed and significant wave height from the ERA-40 data, *J. Clim.*, *18*, 1032–1048.

Cavaleri, L., et al. (2007), Wave modelling—The state of the art, *Prog. Oceanog.*, *75*, 603–674, doi:10.1016/j.pocean.2007.05.005.

Cessaro, R. K. (1994), Sources of primary and secondary microseisms, *Bull. Seismol. Soc. Am.*, *84*(1), 142–148.

Chevrot, S., M. Sylvander, S. Benahmed, C. Ponsolles, J. M. Lefèvre, and D. Paradis (2007), Source locations of secondary microseisms in western Europe: Evidence for both coastal and pelagic sources, *J. Geophys. Res.*, *112*, B11301, doi:10.1029/2007JB005059.

Collard, F., F. Ardhuin, and B. Chapron (2009), Monitoring and analysis of ocean swell fields using a spaceborne SAR: A new method for routine observations, *J. Geophys. Res.*, *114*, C07023, doi:10.1029/2008JC005215.

Cox, C. S., and D. C. Jacobs (1989), Cartesian diver observations of double frequency pressure fluctuations in the upper levels of the ocean, *Geophys. Res. Lett.*, *16*(8), 807–810.

Crombie, D. D. (1955), Theory of HF ground wave backscatter from sea waves, *Nature*, *175*, 681–682.

Delpey, M., F. Ardhuin, F. Collard, and B. Chapron (2010), Space-time structure of long swell systems, *J. Geophys. Res.*, *115*, C12037, doi:10.1029/2009JC005885.

Donelan, M., and W. J. Pierson Jr. (1983), The sampling variability of estimates of spectra of wind-generated gravity waves, *J. Geophys. Res.*, *88*(C7), 4381–4392.

Duennebier, F. K., R. Lukas, E.-M. Nosal, J. Aucan, and R. A. Weller (2012), Wind, waves, and acoustic background levels at station aloha, *J. Geophys. Res.*, *117*, C03017, doi:10.1029/2011JC007267.

Ebeling, C. W., and S. Stein (2011), Seismological identification and characterization of a large hurricane, *Bull. Seismol. Soc. Am.*, *101*(1), 399–403, doi:10.1785/0120100175.

Elgar, S., T. H. C. Herbers, and R. T. Guza (1994), Reflection of ocean surface gravity waves from a natural beach, *J. Phys. Oceanogr.*, *24*(7), 1503–1511.

Essen, H.-H., J. Klussmann, R. Herber, and I. Grevemeyer (1999), Do microseisms in Hamburg (Germany) reflect the wave climate in the North Atlantic?, *Deut. Hydrogr. Z.*, *51*(1), 33–47.

Essen, H.-H., F. Krüger, T. Dahm, and I. Grevemeyer (2003), On the generation of secondary microseisms observed in northern and central Europe, *J. Geophys. Res.*, *108*(B10), 2506, doi:10.1029/2002JB002338.

Fabrikant, A. L., and M. A. Raevsky (1994), The influence of drift flow turbulence on surface gravity wave propagation, *J. Fluid Mech.*, *262*, 141–156.

Farrell, W. E., and W. Munk (2008), What do deep sea pressure fluctuations tell about short surface waves?, *Geophys. Res. Lett.*, *35*, L19605, doi:10.1029/2008GL035008.

Farrell, W. E., and W. Munk (2010), Booms and busts in the deep, *J. Phys. Oceanogr.*, *40*(9), 2159–2169.

Gerstoft, P., and T. Tanimoto (2007), A year of microseisms in southern california, *Geophys. Res. Lett.*, *34*, L20304, doi:10.1029/2007GL031091.

Hanafin, J., et al. (2012), Phenomenal sea states and swell radiation: A comprehensive analysis of the 12-16 February 2011 North Atlantic storms, *Bull. Am. Meterol. Soc.*, in press.

Hasselmann, D. E., M. Dunckel, and J. A. Ewing (1980), Directional wave spectra observed during JONSWAP 1973, *J. Phys. Oceanogr.*, *10*, 1264–1280.

Hasselmann, K. (1963), A statistical analysis of the generation of microseisms, *Rev. Geophys.*, *1*(2), 177–210.

Haubrich, R. A., and K. McCamy (1969), Microseisms: Coastal and pelagic sources, *Bull. Seismol. Soc. Am.*, *7*(3), 539–571.

Herbers, T. H. C., and R. T. Guza (1994), Nonlinear wave interactions and high-frequency seafloor pressure, *J. Geophys. Res.*, *99*, 10,035–10,048.

Holthuijsen, L. H., and H. L. Tolman (1991), Effects of the Gulf Stream on ocean waves, *J. Geophys. Res.*, *96*(C7), 12,755–12,771.

Kedar, S., M. Longuet-Higgins, F. W. N. Graham, R. Clayton, and C. Jones (2008), The origin of deep ocean microseisms in the north Atlantic ocean, *Proc. R. Soc. A*, *464*, 1–35, doi:10.1098/rspa.2007.0277.

Kuik, A. J., G. P. van Vledder, and L. H. Holthuijsen (1988), A method for the routine analysis of pitch-and-roll buoy wave data, *J. Phys. Oceanogr.*, *18*, 1020–1034.

Lavrenov, I. V. (2003a), *Wind-Waves in Oceans: Dynamics and Numerical Simulations*, 376 pp., Springer, Berlin.

Lavrenov, I. V. (2003b), A numerical study of a nonstationary solution of the Hasselmann equation, *J. Phys. Oceanogr.*, *33*, 499–511.

Long, C. E., and D. T. Resio (2007), Wind wave spectral observations in Currituck Sound, North Carolina, *J. Geophys. Res.*, *112*, C05001, doi:10.1029/2006JC003835.

Longuet-Higgins, M. S. (1950), A theory of the origin of microseisms, *Philos. Trans. R. Soc. A*, *243*, 1–35.

Magne, R., K. Belibassakis, T. H. C. Herbers, F. Ardhuin, W. C. O'Reilly, and V. Rey (2007), Evolution of surface gravity waves over a submarine canyon, *J. Geophys. Res.*, *112*, C01002, doi:10.1029/2005JC003035.

Miche, A. (1944), Mouvements ondulatoires de la mer en profondeur croissante ou décroissante. forme limite de la houle lors de son déferlement. application aux digues maritimes. deuxième partie. mouvements ondulatoires périodiques en profondeur régulièrement décroissante, *Ann. Ponts Chaussées*, *114*, 369–406.

Munk, W. H., G. R. Miller, F. E. Snodgrass, and N. F. Barber (1963), Directional recording of swell from distant storms, *Philos. Trans. R. Soc. A*, *255*, 505–584.

O'Reilly, W. C., R. T. Guza, and R. J. Seymour (1999), Wave prediction in the Santa Barbara channel, *Rep. MMS 2001-055*, Miner. Manage. Serv., Santa Barbara, Calif. [Available at http://www.coastalresearchcenter.ucsb.edu/cmi/files/2001-055.pdf.]

Pawka, S. S. (1983), Island shadows in wave directional spectra, *J. Geophys. Res.*, *88*, 2579–2591.

Queffeulou, P. (1983), SEASAT wave height measurement: A comparison with sea-truth data and a wave forecasting model—Application to the geographic distribution of strong sea states in storms, *J. Geophys. Res.*, *88*, 1779–1788.

Saha, S., et al. (2010), The NCEP Climate Forecast System Reanalysis, *Bull. Am. Meterol. Soc.*, *91*, 1015–1057.

Schimmel, M., E. Stutzmann, F. Ardhuin, and J. Gallart (2011), Polarized earth's ambient microseismic noise, *Geochem. Geophys. Geosyst.*, *12*, Q07014, doi:10.1029/2011GC003661.

Schulte-Pelkum, V., P. S. Earle, and F. L. Vernon (2004), Strong directivity of ocean-generated seismic noise, *Geochem. Geophys. Geosyst.*, *5*, Q03004, doi:10.1029/2003GC000520.

Squire, V., J. Duggan, P. Wadhams, P. Rottier, and A. Liu (1995), Of ocean waves and sea ice, *Annu. Rev. Fluid Mech.*, *27*(3), 115–168.

Tournadre, J., and R. Ezraty (1990), Local climatology of wind and sea state by means of satellite radar altimeter measurements, *J. Geophys. Res.*, *95*, 18,255–18,268.

Traer, J., P. Gerstoft, P. D. Bromirski, W. S. Hodgkiss, and L. A. Brooks (2008), Shallow-water seismoacoustic noise generated by tropical storms Ernesto and Florence, *JASA Express Lett.*, *124*(3), EL170–EL176, doi:10.1121/1.2968296.

Webb, S. C., and W. C. Crawford (2010), Shallow-water broadband OBS seismology, *Bull. Seismol. Soc. Am.*, *100*(4), 1770–1778, doi:10.1785/0120090203.

Zhang, J., P. Gerstoft, and P. D. Bromirski (2010), Pelagic and coastal sources of P-wave microseisms: Generation under tropical cyclones, *Geophys. Res. Lett.*, *37*, L15301, doi:10.1029/2010GL044288.

Zopf, D. O., H. C. Creech, and W. H. Quinn (1976), The wavemeter: A land-based system for measuring nearshore ocean waves, *Mar. Tech. Soc. J.*, *10*(4), 19–25.

F. Ardhuin, A. Balanche, and M. Obrebski, Ifremer, Laboratoire d'Océanographie Spatiale, Centre de Brest, B.P. 70, F-29280 Plouzane, France. (ardhuin@ifremer.fr)

E. Stutzmann, Departement de Sismologie, Institut de Physique du Globe, PRES Sorbonne Paris-Cité, F-75005 Paris, France.